375

Ozone-radiation interactions in the ECMWF forecast system

Jean-Jacques Morcrette

Research Department

December 2003

The Library
ECMWF
Shinfield Park
Reading, Berks RG2 9AX

library@ecmwf.int

Series: ECMWF Technical Memoranda

A full list of ECMWF Publications can be found on our web site under:
http://www.ecmwf.int/publications/library/ecpublications/

ABSTRACT

Interactions between radiative processes and the ozone field forecast by the ECMWF system, operational in January 2002, are studied in 19-month T_L159 L60 simulations with the ozone transported by the dynamics of the model, with and without interactions with the radiation schemes. The sensitivity of the model ozone and temperature to the description of the longwave and shortwave radiative transfer is considered. Both the Rapid Radiation Transfer Model and the new 6-interval shortwave scheme contribute to a warmer stratosphere in better agreement with climatology, and a generally colder lower stratosphere in the tropics, this last feature linked to a deficient vertical transport.

Comparisons are also made of 10-day forecasts with and without ozone-radiation interactions. Compared with ERA-40 analyses, the forecasts including the ozone-radiation interactions show relatively small and generally positive impact on the objective scores of temperature at 100, 50, 30 and 10 hPa. Comparing with ozonesonde observations, the forecasts with ozone-radiation interactions do not differ much from those without such interactions. Temperature profiles are generally well analysed, but forecasted ozone is often in slightly better agreement with the observed ozone profiles than the analyzed ozone.

1 Introduction

On 9 March 1999, the forecast system of the European Centre for Medium-range Weather Forecasts (ECMWF) had its highest prognostic level moved from 10 hPa (~ 30km) to 0.1 hPa (~ 65 km). Since 12 October 1999, ozone is a prognostic variable with a simplified representation of chemistry (Cariolle and Deque, 1986). The latest update to the chemistry package (Simon, 2001), now including a representation of heterogeneous chemistry, was introduced on 12 June 2001. It was used in the forty-year reanalysis of meteorological observations (the so-called ERA40), for those years when relevant satellite observations of ozone, usually through measurements of the radiance reflected in the solar spectrum, are available. In the ECMWF model, ozone is one of the prognostic variables, together with surface pressure, temperature, humidity, and components of the wind. Ozone is assimilated in the model following an analysis of the satellite radiances sensitive to ozone (either from the Total Ozone Mapping Spectrometer - TOMS - onboard NASA satellites or the Solar Backscatter UltraViolet instrument - SBUV/2 - onboard NOAA operational polar orbiting satellites). It is then advected by the dynamics of the model, with the sources and sinks represented according to Cariolle et al. (1986). In the operational configuration, this ozone field is not interactive with the radiative calculations. A monthly climatology from Fortuin and Langematz (1994) provides the zonal mean latitude-height distribution of the ozone mixing ratio that is actually used in the radiative computations. Therefore in the operational configuration, ozone is only a weakly interactive tracer, depending mainly on the model dynamics and on temperature through its sources and sinks, but without any direct ozone-radiation interactions and therefore no feedback on the other model fields, either diagnostic or prognostic.

Starting from the 70s, a number of studies addressed the sensitivity of the tropospheric temperature to perturbations in the concentration of ozone in the stratosphere (Ramanathan et al, 1976), and the role of ozone in the energy balance of the stratosphere-troposphere system (Ramanathan and Dickinson, 1979; Kiehl and Boville, 1988). General circulation model simulations including interactive ozone were initiated by Schlesinger and Mintz (1979), Cunnold et al. (1980) and Mahlman et al. (1980) using no or simplified representations of the radiative transfer (RT) processes. Cariolle and Deque (1986) proposed a linearization of the ozone photochemical sources and sinks and the calculation of the relaxation coefficients using a two-dimensional photochemical model (Cariolle and Brard, 1984). The main advantages of such an approach are

its numerical simplicity and the possibility to control its accuracy by comparisons with calculations performed with a sophisticated photochemical model. Such a method, with additional refinements, is in use in both the Meteo-France ARPEGE climate model (Simon, 2001) and in the ECMWF forecast system (Dethof and Holm, 2002).

This study aims at answering a number of questions: Is the present description of ozone, used at ECMWF for 10-day forecasts, able to provide realistic long-term behaviour, when the radiation processes are made interactive with the ozone distribution, and how is the model ozone and temperature dependent on the quality of the representation of the radiative processes? Section 2 briefly describes the parametrisation of the ozone processes, and the versions of the longwave and shortwave radiation schemes used in the sensitivity calculations. To look at the long-term behaviour of the model fields, results of 19-month integrations are presented in section 3. Section 4 discusses the potential impact of a radiatively interactive ozone in analyses and subsequent 10-day forecasts at higher spatial resolution. A summary and discussion are given in section 5.

2 Model configuration and methodology

2.1 Representation of ozone processes

As discussed in Dethof and Holm (2002), the approach used within the ECMWF forecast system for the ozone analysis was originally designed to minimize the effect of ozone on the rest of the model. Ozone is fully integrated into the ECMWF forecast model as an additional three-dimensional variable similar to humidity. The forecast model includes a prognostic equation for ozone mass mixing ratio [kg/kg]

$$dO_3/dt = R_{O3}$$

where R_{O3} is a parametrisation of sources and sinks of ozone. Without such a source/sink parametrisation, the ozone distribution would drift to unrealistic values in integrations longer than a few weeks. This parametrisation must maintain a realistic ozone three-dimensional distribution over several years of integration, without reducing the dynamical variability of ozone. In addition, the parametrisation should be able to create an Antarctic ozone hole when the conditions are right. The parametrisation used in the ECMWF model is an updated version of the ozone scheme originally developed for the ARPEGE climate model at Meteo-France (Cariolle and Deque, 1986; Cariolle et al., 1990). It assumes that chemical changes in ozone can be described by a linear relaxation towards a photochemical equilibrium. As such, it is essentially a stratospheric parametrisation. The reaction rates and the equilibrium values have been determined from a photochemical model, including a representation of the heterogeneous ozone hole chemistry. The updated version of the parametrisation (Simon, 2001) is

$$R_{O3} = c_0 + c_1 (O_3 - \overline{O_3}) + c_2 (T-\overline{T}) + c_3 (O_3^+ - \overline{O}_3^+) + c_4 (Cl_{Eq})^2 O_3$$

$$\text{where } O_3^+ = -\int_p^0 O_3(p')/g \, dp'$$

Here the c_i are the relaxation rates and $\overline{T}$, $\overline{O_3}$, and $\overline{O_3}^+$ are photochemical equilibrium values, all functions of latitude, pressure and month. Cl_{Eq} is the equivalent chlorine content of the stratosphere for the actual year, and is the only parameter that varies from year to year (Dethof and Holm, 2002). For the ECMWF model, the photochemical equilibrium values for ozone are taken from the ozone climatology derived from observations by Fortuin and Langematz (1994). The parametrisation is only active in daylight, and the heterogeneous part is only turned on below a threshold temperature of 195 K. Although the parametrisation is mainly geared

towards the representation of the stratospheric ozone, it is used over the full depth of the atmosphere. Results for the tropospheric ozone are discussed in section 3.

2.2 The longwave radiation schemes: M91/G00 and RRTM

Table 1 presents a summary of the characteristics of the two longwave (LW) schemes used in the following sections. The LW radiation scheme, operational at ECMWF from May 1989 to June 2000 (Morcrette, 1991) accounts for absorption by water vapour, carbon dioxide, ozone, methane, nitrous oxide, CFC-11, and CFC-12. It is based on an emissivity method in which the transmission functions for water vapour and carbon dioxide over the six spectral intervals of the scheme have been fitted using Pade approximants on narrow-band transmissions obtained with statistical band models. At the time of its development, it was validated against the Laboratoire de Meteorologie Dynamique 4A line-by-line model. However, despite some update to the absorption coefficients following the availability of newer versions of the database of spectroscopic parameters (from HITRAN'82 to HITRAN'86 to HITRAN'92), some of its features made it somewhat outdated, particularly its parametrization of the water vapour continuum absorption, based on Roberts et al. (1976). In consequence, a revision of the water vapour continuum based on continuum measurements (CKD1) by Clough et al. (1992) was introduced as part of the December 1997 revision (cycle 18r3) of the physics package (Gregory et al., 2000; hereafter M91/G00). An approximate representation of the Voigt profile of the lines following Giorgetta and Morcrette (1995) is included in the longwave radiation transfer scheme. For the longwave spectral intervals of M91/G00, ice cloud optical properties are derived from Ebert and Curry (1992), and water cloud optical properties from Smith and Shi (1992). In this scheme, semi-transparent clouds are treated using an effective cloud cover, the product of the actual cloud cover by the cloud emissivity computed for the whole LW spectrum.

Table 1: Characteristics of the longwave radiation schemes

	RRTM	M91/G00
Solution of RT Equation	two-stream method	spectral emissivity method
Number of spectral intervals	16	6
Absorbers	H_2O, CO_2, O_3, CH_4, N_2O, CFC11, CFC12, aerosols	H_2O, CO_2, O_3, CH_4, N_2O, CFC11, CFC12, aerosols
Spectroscopic database	HITRAN, 1996	HITRAN, 1992
Absorption coefficients	from LBLRTM line-by-line model	fits on statistical models of transmission
Cloud handling	true cloud fraction	effective cloud fraction CF*ε
Cloud optical properties: method	16-band spectral emissivity	whole spectrum emissivity
Data Ice Clouds Water Clouds	Ebert & Curry, 1992 Smith & Shi, 1992,	Ebert & Curry, 1992 Smith & Shi, 1992
Cloud overlap assumption	maximum-random	maximum-random (maximum & random also possible)
Reference	Mlawer et al., 1997	Morcrette et al., 1986; Morcrette, 1991 Gregory et al., 2000

In June 2001, the Rapid Radiation Transfer Model (RRTM, Mlawer et al., 1997) replaced the M91/G00 scheme in the operational model (Morcrette et al., 2001). As stated in Mlawer et al. (1997), the objective in the development of RRTM has been to obtain an accuracy in the calculation of fluxes and cooling rates consistent with the best line-by-line models. It utilizes the correlated-k method and shows its affiliation to the AER line-by-line model (LBLRTM, Clough et al., 1989, 1992, Clough and Iacono, 1995) through its use of absorption coefficients for the relevant k-distributions derived from LBLRTM. Therefore the k-coefficients in RRTM include the effect of the CKD2.3 water vapour continuum (Clough et al., 1989).

The main point in the correlated-k method is the mapping of the absorption coefficient k(n) from the spectral space (where it varies irregularly with wavenumber n) to the g-space (where g(k) is the probability distribution function, i.e., the fraction of the absorption coefficients in the set smaller than k. The effect of this reordering is a rearrangement of the sequence of terms in the integral over wavenumber in the RTE, which makes it equivalent to what would be done for monochromatic radiation. The accuracy of these absorption coefficients has been established by numerous and continuing high-resolution validations of LBLRTM with spectroscopic measurements, in particular those from the Atmospheric Radiation Measurement program (ARM). Compared to the original RRTM (Mlawer et al., 1997), RRTM_EC was modified to account for cloud optical properties and surface emissivity defined for each of the 16 bands over which spectral fluxes are computed. For efficiency reason, the original number of g-points (256 = 16 x 16) has been reduced to 140. Other changes are the use of the CKD2.3 water vapour continuum (instead of the CKD2.2 version of the original RRTM) and of a diffusivity approximation (instead of the 3-angle integration over the zenith angle used in the original scheme) to derive upward and downward fluxes from the radiances, and the modification of the original cloud random overlapping assumption to include (to the same degree of approximation as used in the operational ECMWF shortwave scheme) a maximum-random overlapping of cloud layers. Optical properties of clouds have been defined for both water and ice clouds in each of the 16 spectral intervals. Results in the following are for optical properties from Ebert and Curry (1992) for ice clouds, and from Smith and Shi (1992) for liquid water clouds. Given the monochromatic form of the RTE, the vertical integration is simply carried out one layer at a time from the top-of-the-atmosphere to the surface to get the downward fluxes. The downward fluxes at the surface are used with the spectral surface emissivities and the surface temperature to get the upward longwave fluxes in each of the 140 sub-intervals. Then the upward fluxes are computed from surface to top.

The LW heating rate profiles given by M91/G00 and RRTM are presented in Figure 1 for a climatological mid-latitude summer profile. Particularly relevant for the following discussion is the decreased cooling in the upper part of the stratosphere brought by RRTM.

2.3 The shortwave radiation schemes: SW4 and SW6

Table 2 presents a summary of the characteristics of the two shortwave (SW) schemes discussed in the following sections. Since May 1989, the operational shortwave radiation scheme in the ECMWF model has been based on the method originally developed by Fouquart and Bonnel (1980). The radiative transfer equation is solved using a two-stream method, with the scattering by clouds and aerosols handled with a Delta-Eddington approximation (Joseph et al., 1976). The transmission functions for water vapour, uniformly mixed gases and ozone are parametrized using Pade approximants. The reflectivity and transmissivity of any layer in the atmosphere accounts for scattering by molecules (Rayleigh scattering), aerosols and clouds, absorption by the radiatively active gases, aerosols and cloud particles, and reflection by the surface. The computation of these reflectivities and transmissivities is carried out separately for the clear-sky and cloudy

fractions of the atmosphere, and the scheme can accommodate the maximum-random (used operationally in the ECMWF model), the maximum or the random cloud overlap assumption (Morcrette and Fouquart, 1986; Morcrette and Jakob, 2000). From May 1989 to June 2000, the operational shortwave radiation scheme represented the radiative transfer using two spectral intervals only (SW2), one covering the ultraviolet and visible (0.25 - 0.69 μm), and the second one covering the whole near-infrared (0.69 - 4.0 μm) part of the solar spectrum. When this shortwave scheme was introduced in the ECMWF model in May 1989, it used absorption coefficients derived from the 1986 version of the HITRAN database of spectroscopic parameters (Rothman et al., 1987). In 1993, the absorption coefficients were updated following the release of the 1992 version of HITRAN (Morcrette, 1993). This version of the SW scheme was used for the ECMWF 15-year re-analysis (ERA-15; Gibson et al., 1997). Tests done within ECMWF and comparisons with observations (Wild et al., 1998; Wild, 1999) had shown that, despite some provision for the spectral averaging of cloud absorption parameters varying over several orders of magnitude within the near-infrared, this 2-spectral interval version of the scheme greatly overestimated the in-cloud absorption and created some spurious anomalous absorption. This problem was largely removed with the 4-spectral interval version of the scheme, where the near-infrared part of the spectrum is distributed within the three intervals 0.69 - 1.19 - 2.38 - 4.0 μm. This 4-spectral interval version of the SW scheme became operational in June 2000. However, for clear-sky radiation, this version of the shortwave scheme still used fits of transmission functions computed with statistical models, over 0.1 μm-wide intervals, and without any provision for water vapour continuum absorption. The SW2 and M91 LW schemes were used in the studies of the polar ozone holes by Knudsen et al. (1998a, b).

Table 2: Characteristics of the shortwave radiation scheme

	SW6	SW
Solution of RT Equation	Two-stream method	Two-stream method
Number and limits of spectral intervals	0.185 - 0.25 - 0.40 0.69 - 1.19 - 2.38 - 4.0	0.25 - 0.69 - 4.0 0.25 - 0.69 - 1.19 - 2.38 - 4.0
Absorbers	H_2O, CO_2, O_3, O_2, CH_4, N_2O, aerosols	H_2O, CO_2, O_3, O_2, CH_4, N_2O, aerosols
Spectroscopic database	HITRAN, 2000	HITRAN, 1992
Absorption coefficients	Fits on a line-by-line model of the transmission functions	Fits on statistical models of the transmission functions
Cloud optical properties	σ_a , ω, g, in each interval	σ_a , ω, g, in each interval
Data Ice clouds Water clouds	Ebert and Curry, 1992 Fouquart, 1987	Ebert and Curry, 1992 Fouquart, 1987
References	Dubuisson et al., 1996 for line-by-line model	Fouquart and Bonnel, 1980 Morcrette, 1991, 1993

Requirements for a more detailed spectral description of the shortwave radiation in the ECMWF model recently emerged. First, the tiling scheme for surface processes can now use a properly defined photosynthetically active radiation (PAR). Second, as the ECMWF model has moved its top level from 10 to 0.1 hPa, a proper representation of the temperature above 10 hPa requires a proper distribution over the vertical of the radiative heating rate, a requirement which cannot be satisfied by the one spectral interval used

up to now to deal with the ultraviolet and visible parts of the solar spectrum. The availability of revised versions of the HITRAN database (Rothman et al., 1996, 2001), and of line-by-line models of the transmission in the shortwave spectrum (Dubuisson et al., 1996) permits a revisit of the parametrisation of the gaseous absorption within the ECMWF shortwave scheme. As discussed in Dubuisson et al. (1996), the line-by-line model is based on Scott (1974), with a number of modifications to make it compatible to computations in the shortwave part of the spectrum. It includes the gaseous absorption by H_2O, CO_2, O_2, CH_4, N_2O, CO, and O_3 (lines and continuum if present). The water vapour continnum (CKD2.4) follows Clough et al. (1989). All transmission functions were computed with the above line-by-line model using spectroscopic data from HITRAN 2000, with a resolution of about 0.01 cm^{-1} from 2500 to 20000 cm^{-1}, then 5-10 cm^{-1} depending on the data for the O_3 continuum. These transmission functions are then fitted using Pade approximants for use in the parametrisation. Results of this line-by-line model (for the absorption processes) coupled to the discrete ordinate radiative transfer (DISORT) method of Stamnes et al. (1988) (for the scattering processes) are part of the ICRCCM-3 comparison (Barker and Stephens, 2001). The optical thickness for Rayleigh scattering, previously specified in each spectral interval in the SW2/4 scheme, was also made dependent on the cosine of the solar zenith angle. Finally, all other parameters of importance for the shortwave radiation transfer having a potential spectral dependence (aerosol and cloud optical properties, surface albedo) have been recomputed for the six intervals of the scheme. In the process, new sets of optical properties for both liquid and ice water clouds have been added to the scheme. However, for this study, in both SW4 and SW6, the cloud optical properties (optical thickness, assymetry factor and single scattering albedo) are derived from Fouquart (1987) for the liquid water clouds, and from Ebert and Curry (1992) for the ice clouds. Finally, this new version of the SW scheme allows a diagnostic of the ultraviolet radiation reaching the surface. The SW heating rate profile for a climatological mid-latitude summer profile with a cosine of the solar zenith angle of 0.8 is presented in Figure 2 for both SW4 and SW6. The main impact is an additional heating for pressures lower than 10 hPa.

2.4 Experimentation

The individual model configurations used in this study are presented in Table 3. The impact of the various improvements to the ozone-radiation representation in the model can be studied from differences between simulations as detailed in Table 4. First, distinction is made between cases for which the prognostic ozone is non-interactive with the radiation fields (DynOnly), and cases where interaction between the prognosed ozone and radiation transfer is active (RadInter), allowing the impact of having radiation processes computed from the actual ozone distribution prognosed by the model to be assessed. Second, by comparing SW6 and SW4, one can see the impact of a better representation of the ozone absorption including Voigt line broadening in the shortwave. Thirdly, the impact of an improved representation of the longwave radiation transfer, particularly with respect to a representation of CO_2 and ozone absorption including a better handling of the Voigt line profile and more recent spectroscopic information, is seen by comparing RRTM and M91/G00 simulations.

Table 3: Configuration of the individual simulation experiments

Configuration Acronym	Interaction Ozone/ Radiation	Shortwave Radiation Scheme	Longwave Radiation Scheme	ID
R6R	RadInter	SW6	RRTM	e7ys
D6R	DynOnly	SW6	RRTM	e7yq
D4R	DynOnly	SW4	RRTM	e7yr
D6O	DynOnly	SW6	M91/G00	e7zj
R4R	RadInter	SW4	RRTM	e7yt
R6O	RadInter	SW6	M91/G00	e7zl

Table 4: Characterisation of sensitivity from given pairs of simulations

	Objective
R6R-D6R	Impact of ozone-radiation interactions with improved radiation schemes
D6R-D4R	Impact of improved SW on operational ECMWF model configuration
D6R-D6O	Impact of improved LW on operational ECMWF model configuration
R6R-R4R	Impact of improved SW in ozone-radiation interactive simulations
R6R-R6O	Impact of improved LW in ozone-radiation interactive simulations

Two sets of simulations were run. The first set is used for studying the long-term behaviour of the ECMWF model and its sensitivity to ozone-radiation interactions, and includes all possible configurations. In section 3, we report results from these 19-month T_L159 L60 simulations, which are long enough for pinpointing possible spurious trends in the model. Finally, the impact of the ozone-radiation interaction on the quality of 10-day T_L159 L60 forecasts carried out with the R6R and D6R configurations is shown in section 4.

3 Impact on multi-month simulations

Results from the 19-month long simulations have been processed in terms of monthly mean zonal means or time-series for various zones over the whole length of the simulations. Temperature and ozone distributions are discussed in the following. Results are first presented for the simulation for which the prognostic ozone is interactive with the radiation. Discussion focusses on the impact of the new longwave and shortwave scheme, before considering the differences between the interactive and dynamic-only ozone integrations. Emphasis is put on features prevailing during most of the 19-month period, as any modification to the model physics tends to generate some rather different signals (presence or absence of stratospheric warming at high latitudes in particular), which might not be highly statistically significant.

3.1 Annual cycle

Figure 3 presents the time-series of the ozone distribution simulated with the R6R configuration (ozone-radiation interactions are active) averaged over three areas (90°N-60°N, 30°N-30°S, and 60°S-90°S), whereas Figure 4 presents the corresponding temperature distribution. From these figures, the model appears stable and does not show any particular trend. Although 19 months might be too short to characterize the climatological behaviour of the model, this stability is positive. For the 60°N-90°N area, the maximum in the ozone distribution (given in pressure unit, up to 350 mPa) occurs around 60hPa and in April. The maximum ozone is located around 20 hPa over the tropical region, with much smaller temporal variation. Over the southern polar latitudes, the maximum ozone is around 60 hPa and occurs during August. For temperature, the maximum occurs at the stratopause (around 1 hPa) for all latitude bands. The maximum reachs 288 K during the months of June for the northern polar latitudes, fluctuates between 268 and 273 K in the tropical area, and is up to 293 K in January over the southern polar latitudes. The temperature field (Fig. 4) displays the signature of stratospheric warmings in April in the northern polar latitudes and October in the southern polar latitudes. The minimum temperature drops to just below 195 K in the northern polar latitudes around 20 hPa in January, and in the tropical area around 80 hPa from December to March. In the southern polar latitudes, the temperature minimum is below 185 K between 40 and 15 hPa in late July-early August, a temperature well below the 195 K threshold under which polar stratospheric clouds have been found to appear.

3.2 Sensitivity to the longwave radiation representation: D6R-D6O and R6R-R6O

The time-series of the temperature differences in the same three areas is presented in Figure 5, for simulations D6R-D6O, illustrating the impact of RRTM vs M91/G00 when radiation is computed from climatological ozone. Figure 6 presents similar temperature fields but for radiation interactive with the prognosed ozone (R6R-R6O). Features present in both sets of figures are the warming brought by RRTM to the upper stratosphere (between 10 hPa and the top of the model at 0.1 hPa), with a cooling in the lower part of the stratosphere (between 15 hPa and the tropopause), at all latitudes over most of the length of the forecasts. In the tropics (Figs. 5 and 6, middle panels), RRTM brings a warming from 500 hPa upward to the tropopause. The upper stratospheric warming cannot be directly explained by a reduction of the instantaneous longwave cooling rate by RRTM. A more likely explanation is that the warming of the upper tropospheric tropical layers through radiative destabilisation and subsequent increased convective heating, and the cooling of the lower stratosphere produces a increment of radiative energy (in terms of upward longwave radiation at the tropopause level) to be absorbed in the tropical stratosphere. This relative heating is then exported to higher latitudes by the dynamics.

At high latitudes (90°N-60°N and 60°S-90°S), over the general pattern of upper stratospheric warming and lower stratospheric cooling, are superimposed strong features of heating or cooling, of the order of 10 to 20 days, appearing at the end of the local winter season. The length of the phenomena is likely to be distorted (spuriously lenghtened) by the chosen 240-hour post-processing of the model fields in these 19-month simulations.

3.3 Sensitivity to the shortwave radiation representation: D6R-D4R and R6R-R4R

Figures 7 and 8 present similar time-series of the temperature differences as in Figs. 5 and 6, but for simulations D6R-D4R and R6R-R4R. Here the warming impact of the increased absorption by ozone in the SW6 shortwave scheme is seen at all latitudes, in the upper stratosphere when the sun is present. Heating in excess of 5 K is found in the upper stratospheric layers (from 80 hPa up to the top of the model) in the tropics,

in excess of 6 K in the Northern hemisphere high latitudes (from 30 hPa to the model top), in excess of 5 K in the uppermost layers of the Southern hemisphere high latitudes. In contrast to the impact of a change of longwave radiation scheme, the tropospheric impact is almost negligible in the tropics, showing the small impact of the increase in the number of shortwave spectral intervals on the water vapour absorption.

3.4 Impact of ozone-radiation interactions: R6R-D6R

The time-series of the differences in ozone and temperature distributions are presented in Figures 9 and 10, respectively, for the same three zones, for the simulations R6R-D6R, showing the impact of ozone-radiation interactions relative to radiation based on climatological ozone. Both simulations are performed using the more recent RRTM longwave scheme and SW6 shortwave scheme. Making the prognostic ozone interactive with radiation generally leads to a decrease in ozone in the lower stratosphere at high latitudes (Northern hemisphere in top panel, Southern hemisphere in bottom panel) and to a corresponding increase in tropospheric ozone at high latitudes. In the tropics, there is a tropospheric decrease in ozone, mainly located under the tropopause, and a slight increase above. Apart from this impact on ozone for pressures higher than 50 hPa, the main result is the very small impact of temperature differences on the resulting ozone field. In the 90-60^{o}N area, only the large temperature perturbation in the high stratosphere around 6000 hours appears to be able to impact the ozone field. Otherwise all fluctuations in ozone in the tropical and South hemisphere areas for pressure below 50 hPa are below the 5 percent range.

However, the impact on temperature of having radiation interactive with the prognostic ozone is to further decrease the temperature between 100 and 50 hPa in the tropical area. To get an explanation on this additional cooling, Figure 11 compares for July conditions the zonal mean distribution of the prognostic ozone for R6R (top) and D6R (bottom) with the corresponding Fortuin-Langematz ozone climatology. In both cases, whether radiation is interactive or not with the prognostic ozone, the main signal is a large relative decrease of the ozone concentration in the lower stratosphere (between levels 24 and 28), an area normally prone to small shortwave and longwave radiative heating rates. A decrease in the ozone amount above the tropopause leads to a decrease in relative heating by absorption of longwave radiation, therefore to a cooling of this area, and a slight increase in ozone concentration. The fact that the prognostic ozone concentration is at those heights smaller than the climatological values is thought to be linked to a deficient vertical advection.

4 Impact on 10-day forecasts

In seasonal and annual simulations, the interaction between ozone and radiation processes has some impact on both the temperature and the ozone field. A large number of T_L159 L60 forecasts was run with and without ozone-radiation interactions for three periods (January-March 1991, January-March 1992, August-October 1993) from ERA40 initial conditions. In the following, all objective scores from the forecasts are computed with reference to the ERA-40 reanalysis, which does not include ozone-radiation interactions as part of its first-guess forecasts. Most results presented in the following are for the August-October 1993 period, as the impact of the ozone-radiation interactions for the two January-March periods are very similar.

Figures 12 to 15 present the mean temperature error in the upper atmosphere (at 100, 50, 30 and 10 hPa) between the analyzed and forecasted temperature for two three month periods (January to March 1992 in Figures 12 and 13, August to October 1993 in Figures 14 and 15). The model temperature is from 10-day forecasts with the T_L159 L60 model including or not interactions between the radiation schemes and the prognostic ozone. The first result to note is the small impact of the ozone-radiation interactions on the

temperature field during the first 12 hours of the forecasts. In these conditions, and given the small dependence of the ozone field on the temperature field, already noted in section 3.4, analyses performed with and without the ozone-radiation interactions would be very similar in terms of the ozone field. For the 10-day forecasts, the impact of having the ozone-radiation interaction is a systematic cooling of all areas (Northern and Southern hemispheres, and the 20^{o}N-20^{o}S tropical area) at 100 and 50 hPa, a general cooling at 30 hPa (except for the August-October period in the Northern hemisphere), and a heating of all areas in both periods at 10 hPa and higher altitudes. Interestingly, these effects are rather systematic and their signature can be found over the two three-month periods. Whether the impact of the O_3-radiation interactions is positive or not greatly varies: For all heights, and taking ERA-40 analyses as the reference, the cooling is generally a positive feature in both the Northern and Southern hemispheres, generally a rather negative one over the tropics.

Figures 16 and 17 present the anomaly correlation of the geopotential (at 100, 50, 30 and 10 hPa) for the August to October 1993 period. The impact of the ozone-radiation interactions is either negligible or small: it is positive for the Northern hemisphere and tropics at 50 hPa, Northern, Southern hemispheres and tropics at 10 hPa.

5 Comparisons with ozonesonde measurements

Comparisons of observed temperature and ozone profiles, with either analyzed or after a 240-hour forecasts, were performed for stations carrying out regular ozonesonde measurements. Table 5 gives the locations of the stations used in these comparisons.

Table 5: Location of the ozonesonde profiles used for model validation over the August-October 1993 period.

Station	Latitude	Longitude
Alert	82.50	-62.30
Ny Alesund	78.93	11.88
Aberystwyth	52.70	-4.10
Hohenpeissenberg	47.80	11.00
Payerne	46.80	6.95
Laramie	41.30	-105.60
Hilo	19.72	155.08
Lauder	-45.04	169.68
Dumont D'Urville	-66.41	140.01
Georg von Neumayer	-70.65	-8.26
McMurdo	-77.85	166.67
South Pole	-89.90	-24.80

Figures 18 to 23 present these comparisons at Ny Alesund (Fig. 18), Hawaii (Fig. 19), Lauder (Fig. 20), Georg von Neumayer (Fig. 21), McMurdo (Fig. 22) and South Pole (Fig. 23) for some dates during the August-October 1993 period. Table 5 gives the locations of the stations used. A good agreement is generally obtained

for all stations between the observed and analysed temperature profiles. The agreement somewhat degrades later in the forecast, with discrepancy as high as 5 to 10 K after 10 days over the height range covered by the sounding. For the higher stratosphere not covered by the sounding, there is a systematic change in temperature profile from the analyzed to the 10-day final forecasts profiles. The forecast profiles are always smoother, with a broader temperature maximum at the stratopause. Over all the cases studied, the impact of the ozone-radiation interactions is small with the forecast temperature profiles remaining close to each other and sometimes departing widely from the analysed one.

For ozone, the situation is quite different, with the analysed profile often quite different from the observations. The ozone analysis captures the peak in partial pressure around 50 hPa if it is unimodal, and generally overestimates the ozone in the lower troposphere. This is not surprising given the univariate analysis method based on a single visible measurement and specified (and potentially inadequate) structure function on the vertical. The problem remains relatively benign in the summer hemisphere and at low and middle latitudes. It is particularly marked at high latitudes during winter when the observed ozone distribution often displays multiple peaks and an overall reduced ozone amount. In these cases (Figs. 21 to 23), the analysis often mislocates the position and the amplitude of the maximum, generally decreases the ozone to zero below that maximum and overestimates the lower tropospheric ozone. The ozone profiles after a 240-hour forecast do not depend whether the ozone-radiation interactions are considered or not. They suffer from the same deficiencies as the analysed profiles, although they do not display any drop to zero below the maximum peak of the distribution.

6 Summary and discussion

In this study, the impact of having the radiation processes interactive with the prognostic ozone has been studied. The role of a better representation of the longwave and shortwave radiative processes was studied by comparing 19-month simulations including various versions of the radiation schemes, without and with ozne-radiation interactions. The main impact of the RRTM longwave scheme and of the six-interval shortwave scheme is a warming of the upper atmosphere, in better agreement with the climatology.

The ozone field is prognosed following a revised version of the scheme by Cariolle and Deque (1986). It shows a good stability in year-long simulations, smoother and more consistent when radiation is interactive with ozone. This ozone representation has only a small dependence on local temperature, which translates into an absence of interaction with the troposphere.

In 10-day forecasts, the temperature in the lower stratosphere is modified depending whether ozone-radiation interactions are taken into account or not, with a generally positive but small impact on objective scores of temperature and geopotential.

Comparisons with observed temperature and ozone profiles corroborate some well-known shortcomings of the ozone parametrisation. In winter months, there is a 'severe' overestimation of ozone poleward of 50^{o} when there are no ozone observations in a framework where the wind and temperature are given by assimilated observations. Candidates range from too strong chemistry in the tropics to transport imbalances, possibly caused by biased satellite radiances. When radiation is made interactive with the prognostic ozone, a further cooling appears above the tropopause in the lower stratosphere, linked to a smaller local concentration of the prognostic ozone w.r.t. to the climatological values of ozone used when radiation is not interactive.

When comparing with ozonesonde measurements, the deficiencies seen in the ozone concentration in the lowest levels have been partly addressed by Dethof and Holm in a retuning of the structure function for ozone, now used in the operational forecast model.

Acknowledgments:

Drs Dubuisson and Bonnel (LOA, Lille, France) are thanked for providing the absorption coefficients used within the six-spectral-interval version of the shortwave code. Drs Mlawer, Iacono, and Clough (AER, Inc.) provided the RRTM longwave radiation code, now operational in the ECMWF forecast system. At ECMWF, Drs A. Dethof, E.V. Holm and A. Untch are thanked for help in setting the experimentation and discussing some of the results. Dr A. Simmons provided the code for verifying the forecast against the ERA40 reanalysis and C. Gibert helped with plotting some of the objective scores. Drs A. Hollingsworth, M. Miller and A. Beljaars and A. Untch are thanked for their comments on the manuscript.

References

Barker, H.W., and G.L. Stephens, 2001: An intercomparison of 1-D solar radiative transfer codes: from simple to complex cloudy atmospheres. GEWEX Newsletter 11, 3, 7-10.

Cariolle, D., and D. Brard, 1984: The distribution of ozone and active stratospheric species: Results of a two-dimensional atmospheric model, in Atmospheric Ozone, C.S. Zerefos and A. Ghazi, eds., D. Reidel, Higham, Mass., 77-81.

Cariolle, D., and M. Deque, 1986: Southern hemisphere medium-scale waves and total ozone disturbances in a spectral general circulation model. J. Geophys. Res., 91, 10825-10846.

Cariolle, D., M. Deque, and J.-J. Morcrette, 1986: A GCM simulation of the ozone seasonal variations at high latitudes in the Southern hemisphere. Geophys. Res. Letters, 13, 1304-1307.

Cariolle, D.A., A. Lasserre-Bigorry, J.-F. Royer, and J.-F. Geleyn, 1990: A general circulation model simulation of the springtime Antarctic ozone decrease and its impact on midlatitudes. J. Geophys. Res., 95D, 1883-1898.

Cunnold, D.M., F. Alyea, and R.G. Prinn, 1980: Preliminary calculations concerning the maintenance of the zonal mean ozone distribution in the northern hemisphere. Pure Appl. Geophys., 118, 329-354.

Dethof, A., and E. V. Holm, 2002: Ozone in ERA-40: 1991-1996. ECMWF Technical Memorandum No. 377, August 2002, 37 pp.

Dubuisson P., J.C. Buriez and Y. Fouquart,1996: High Spectral Resolution Solar Radiative Transfer in Absorbing and Scattering Media: Application to the Satellite Simulation, J. Quant. Spectrosc. Radiat. Transfer, 55, 103-126.

Ebert, E.E., and J.A. Curry, 1992: A parametrisation of ice cloud optical properties for climate models. J. Geophys. Res., 97D, 3831-3836.

Fortuin, J. P. F. and U., Langematz, 1994: An update on the global ozone climatology and on concurrent ozone and temperature trends. Proceedings SPIE Vol. 2311, Atmospheric Sensing and Modeling, 207-216.

Fouquart, Y., 1987: Radiative transfer in climate models. NATO Advanced Study Institute on Physically-Based Modelling and Simulation of Climate and Climatic Changes. Erice, Sicily, 11-23 May 1986. M.E. Schlesinger, Ed., Kluwer Academic Publishers, 223-284.

Fouquart, Y., and B. Bonnel, 1980: Computations of solar heating of the earth's atmosphere: a new parameterization. Beitr. Phys. Atmosph., 53, 35-62.

Giorgetta, M.A., and J.-J. Morcrette, 1995: Voigt line approximation in the ECMWF radiation scheme. Mon. Wea. Rev., 123, 3381-3383.

Gregory, D., J.-J. Morcrette, C. Jakob, and A.C.M. Beljaars, and T. Stockdale, 2000: Revision of convection, radiation, and cloud schemes in the ECMWF integrated forecasting system. Quart. J. Roy. Meteor. Soc., 126A, 1685-1710.

Kiehl, J.T., and B.A. Boville, 1988: The radiative-dynamical response of a tropospheric-stratospheric general circulation model to changes in ozone. J. Atmos. Sci., 45, 1798-1817.

Knudsen, B.M., A. Lahoz, A. O'Neill, and J.-J. Morcrette, 1998: Evidence for a substantial role for dilution in Northern mid-latitude ozone depletion. Geophys. Res. Letters, 25, 4501-4504.

Knudsen, B.M., N. Larsen, I.S. Mikkelsen, J.-J. Morcrette, G.O. Braathen, E. Kyro, H. Fast, H. Gernandt, H. Kanzana, H. Nakane, V. Dorokhov, V. Yushkov, G. Hansen, M. Gil, and R.J. Shearman, 1998: Ozone depletion in and below the Arctic vortex for 1997. Geophys. Res. Letters, 25, 627-630.

Mahlman, J.D., H. Levy, II, and W.J. Moxin, 1980: Three-dimensional tracer structure and behavior as simulated in two ozone precursor experiments. J. Atmos. Sci., 37, 655-684.

Mlawer, E.J., S.J. Taubman, P.D. Brown, M.J. Iacono, and S.A. Clough, 1997: Radiative transfer for inhomogeneous atmospheres: RRTM, a validated correlated-k model for the longwave. J. Geophys. Res., 102D, 16,663-16,682.

Morcrette, J.-J., 1991: Radiation and cloud radiative properties in the ECMWF operational weather forecast model. J. Geophys. Res., 96D, 9121-9132.

Morcrette, J.-J., 1993: Revision of the clear-sky and cloud radiative properties in the ECMWF model. ECMWF Newsletter, 61, 3-14.

Morcrette, J.-J., and C. Jakob, 2000: The response of the ECMWF model to changes in cloud overlap assumption. Mon. Wea. Rev., 128, 1707-1732.

Morcrette, J.-J., E.J. Mlawer, M.J. Iacono, and S.A. Clough, 2001: Impact of the radiation transfer scheme RRTM in the ECMWF forecasting system. ECMWF Newsletter, 91, 2-9.

Morcrette, J.-J., L. Smith, and Y. Fouquart, 1986: Pressure and temperature dependence of the absorption in longwave radiation parameterizations. Beitr. Phys. Atmosph., 59, 455-469.

Ramanathan, V., L.B. Callis, and R.E. Boughner, 1976: Sensitivity of surface temperature and atmospheric temperature to perturbations to the stratospheric concentration of ozone and nitrogen dioxide. J. Atmos. Sci.,33, 1092-1112.

Ramanathan, V., and R.E. Dickinson, 1979: The role of stratospheric ozone in the zonal and seasonal radiative energy balance of the earth-troposphere system. J. Atmos. Sci., 36, 1084-1104.

Scott, N.A., 1974: A direct method for computation of the transmission function of an inhomogeneous gaseous atmosphere. Part I: Description of the method. J. Quant. Spectrosc. Radiat. Transfer, 14, 691-704.

Schlesinger, M.E., and Y. Mintz, 1979: Numerical simulation of ozone production, transport and distribution with a global atmospheric general circulation model. J. Atmos. Sci., 36, 1325-1361.

Simon, P., 2001: personal communication

Smith, E. A., and Lei Shi, 1992: Surface forcing of the infrared cooling profile over the Tibetan plateau. Part I: Influence of relative longwave radiative heating at high altitude. J. Atmos. Sci., 49,805-822.

Stamnes, K., S.-C. Tsay, W. Wiscombe, and K. Jayaweera, 1988: Numerically stable algorithm for discrete-ordinate-method radiative transfer in multiple scattering and emitting layered media. Appl. Opt., 27, 2502-2509.

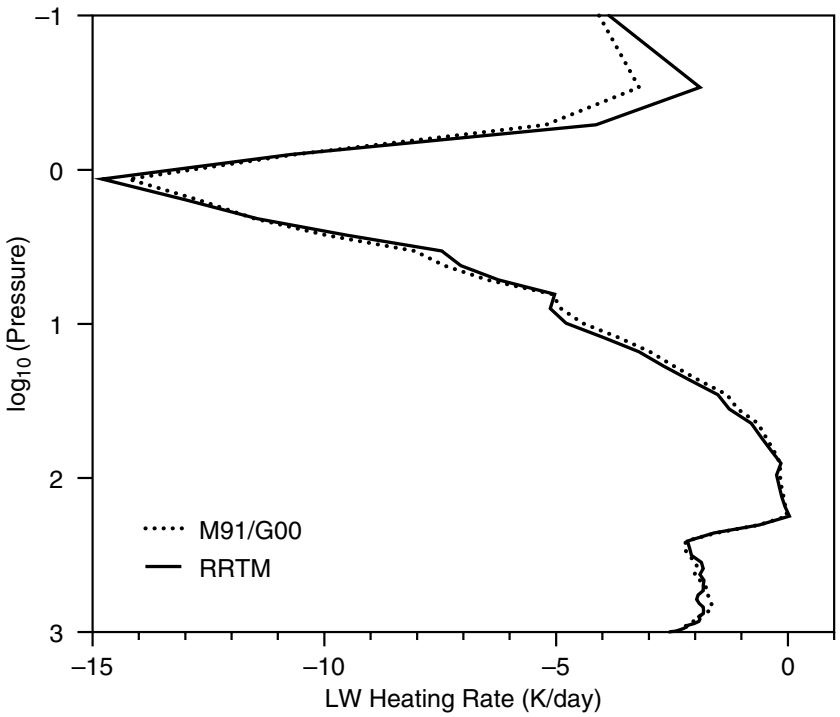

Figure 1 : The longwave radiative heating rate computed for the mid-latitude summer standard atmosphere by the M91/G00 and RRTM longwave radiation schemes.

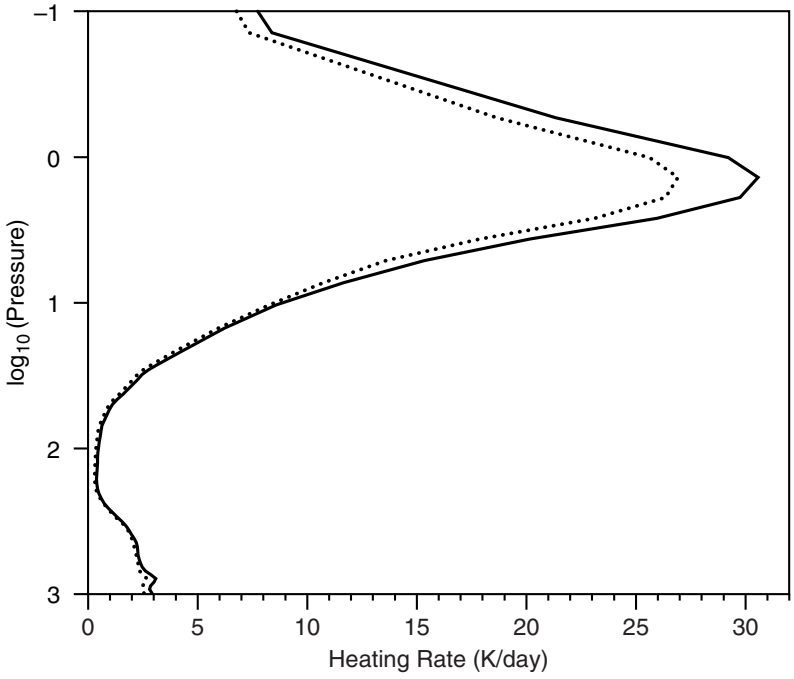

Figure 2 : The shortwave radiative heating rate computed for the mid-latitude summer standard atmosphere by the four- and six-interval versions of the shortwave radiation scheme.

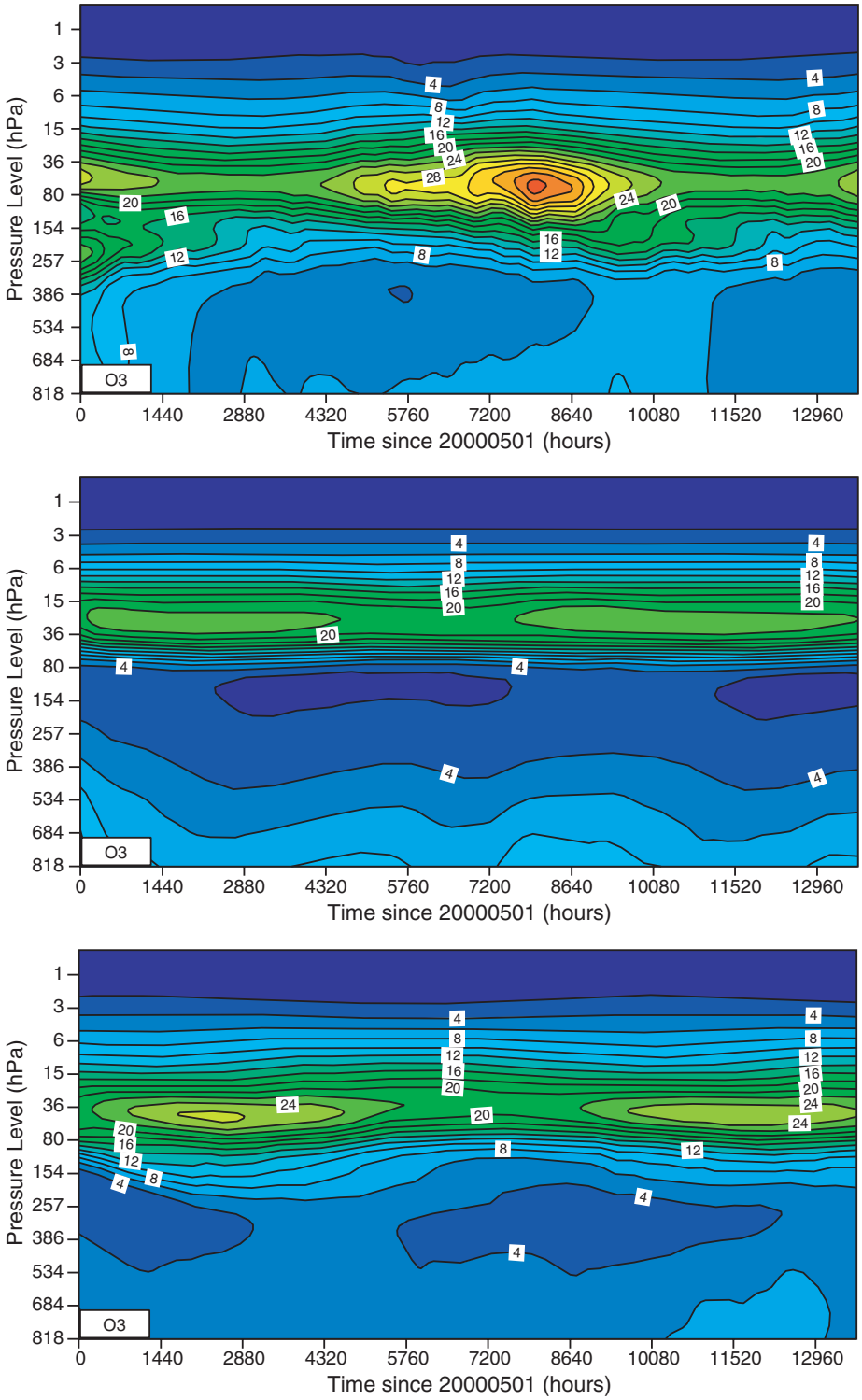

Figure 3 : The time-series of the ozone distribution (R6R) over the zones 90°N-60°N (top), 30°N-30°S (middle) and 60°S-90°S (bottom). Results are with the T_L159 L60 model running for 19 months from 20000501, with the prognostic ozone interactive with the radiation calculations. Unit is mPa.

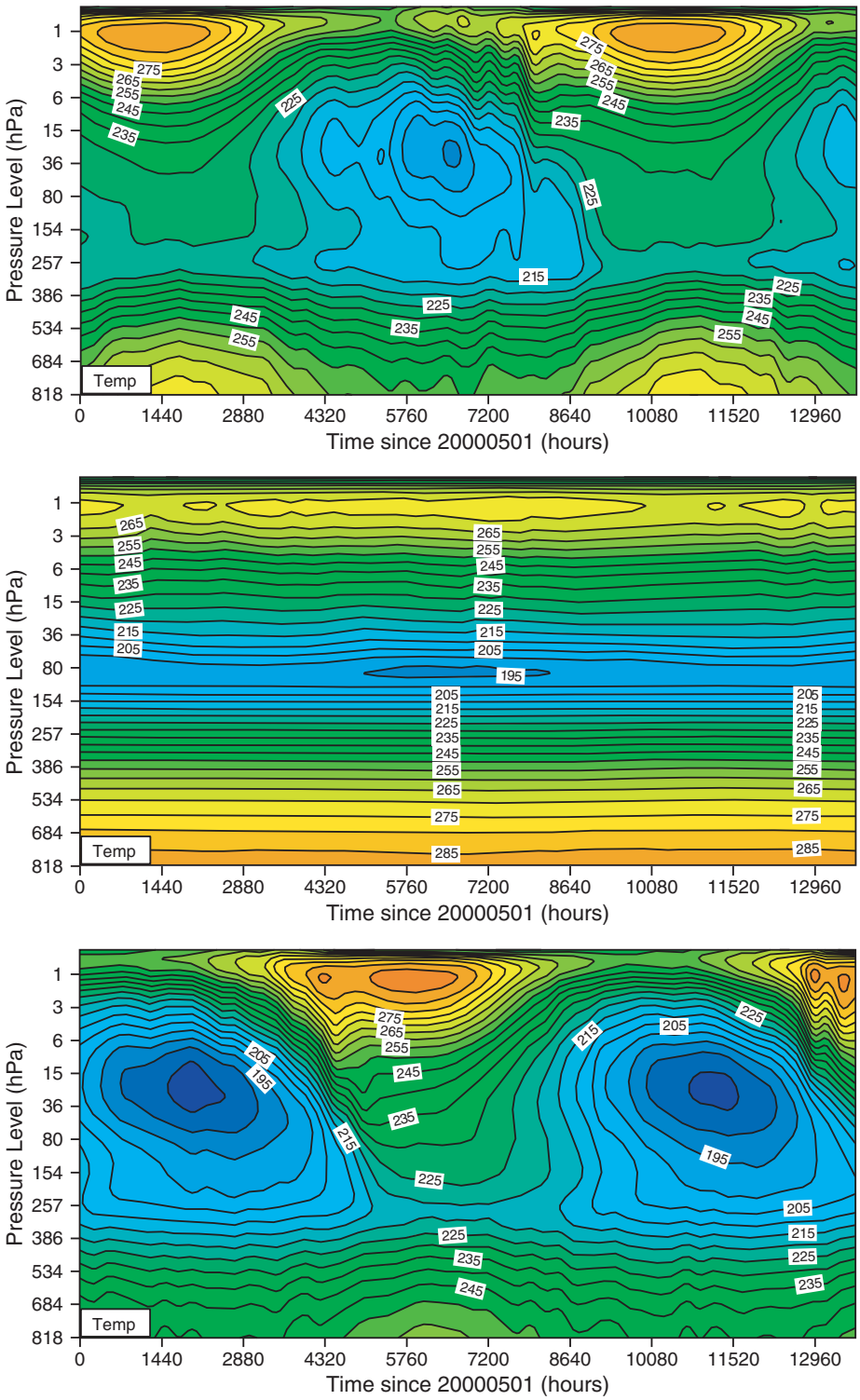

Figure 4 : The time-series of the temperature distribution (R6R) over the zones 90°N-60°N (top), 30°N-30°S (middle) and 60°S-90°S (bottom). Results are with the T_L159 L60 model running for 19 months from 20000501, with the prognostic ozone interactive with the radiation calculations. Unit is degree K.

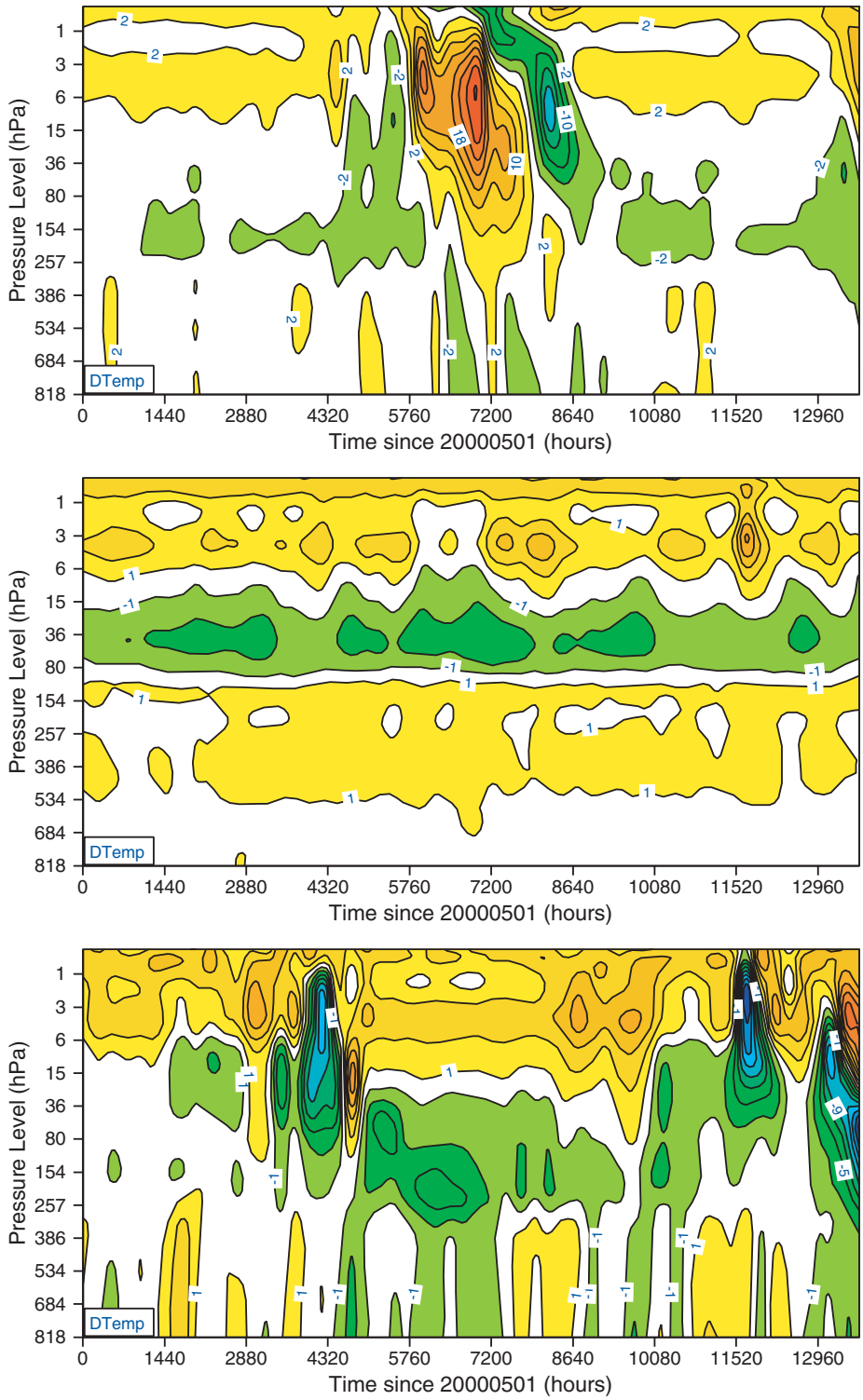

Figure 5 : The time-series of the differences (D6R-D6O) in temperature distribution over the zones 90°N-60°N (top), 30°N-30°S (middle) and 60°S-90°S (bottom) due a different longwave radiation scheme. Results are with the T_L159 L60 model running for 19 months from 20000501, with the radiation calculations from a climatological ozone field. Unit is degree K.

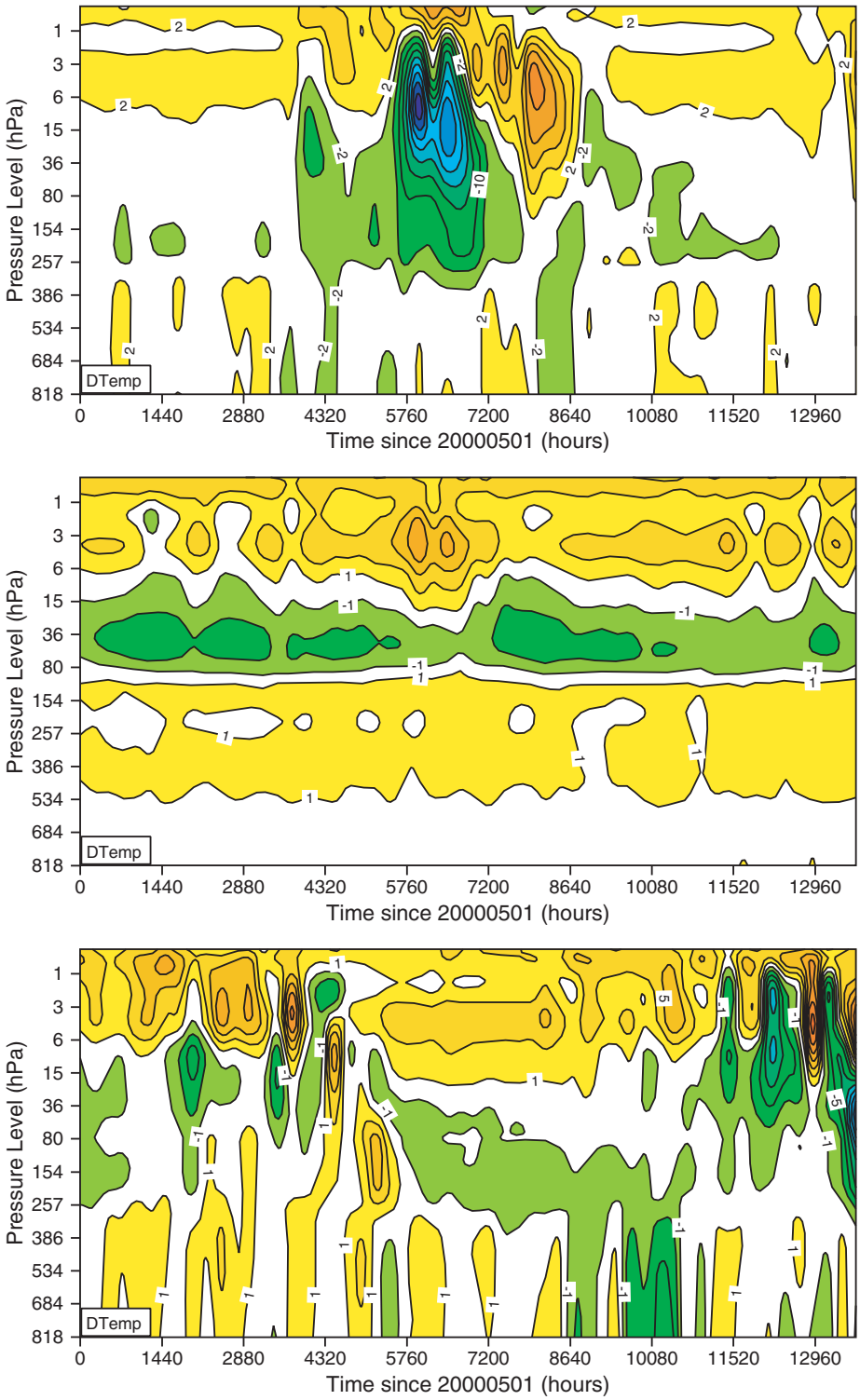

Figure 6 : The time-series of the differences (R6R-R6O) in temperature distribution over the zones 90°N-60°N (top), 30°N-30°S (middle) and 60°S-90°S (bottom), due to a different longwave radiation scheme. Results are with the T_L159 L60 model running for 19 months from 20000501, with the radiation calculations interactive with the prognostic ozone. Unit is degree K.

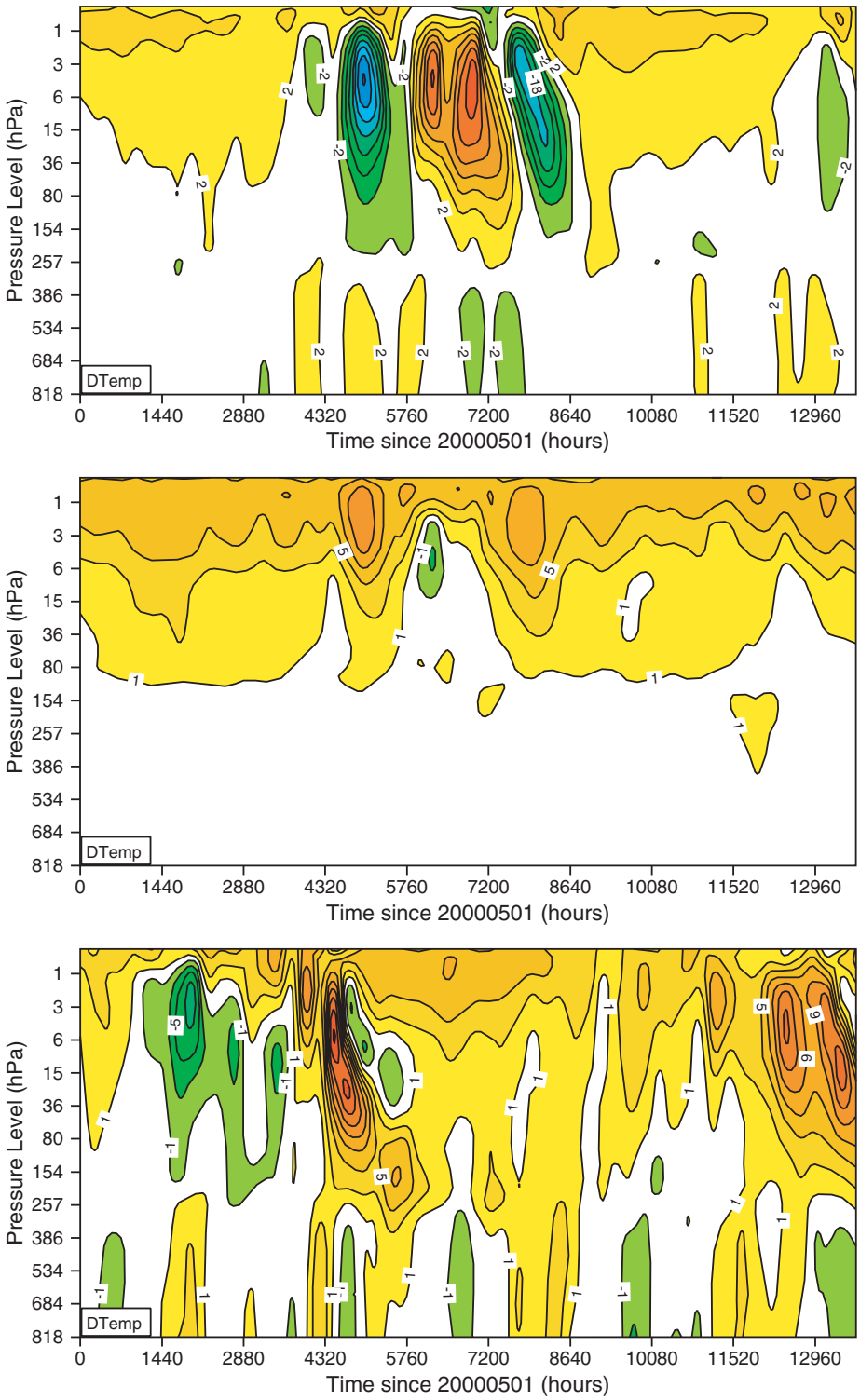

Figure 7 : The time-series of the differences (D6R-D4R) in temperature distribution over the zones 90°N-60°N (top), 30°N-30°S (middle) and 60°S-90°S (bottom), due to a different shortwave radiation scheme. Results are with the T_L159 L60 model running for 19 months from 20000501, with the radiation calculations from a climatological ozone field. Unit is degree K.

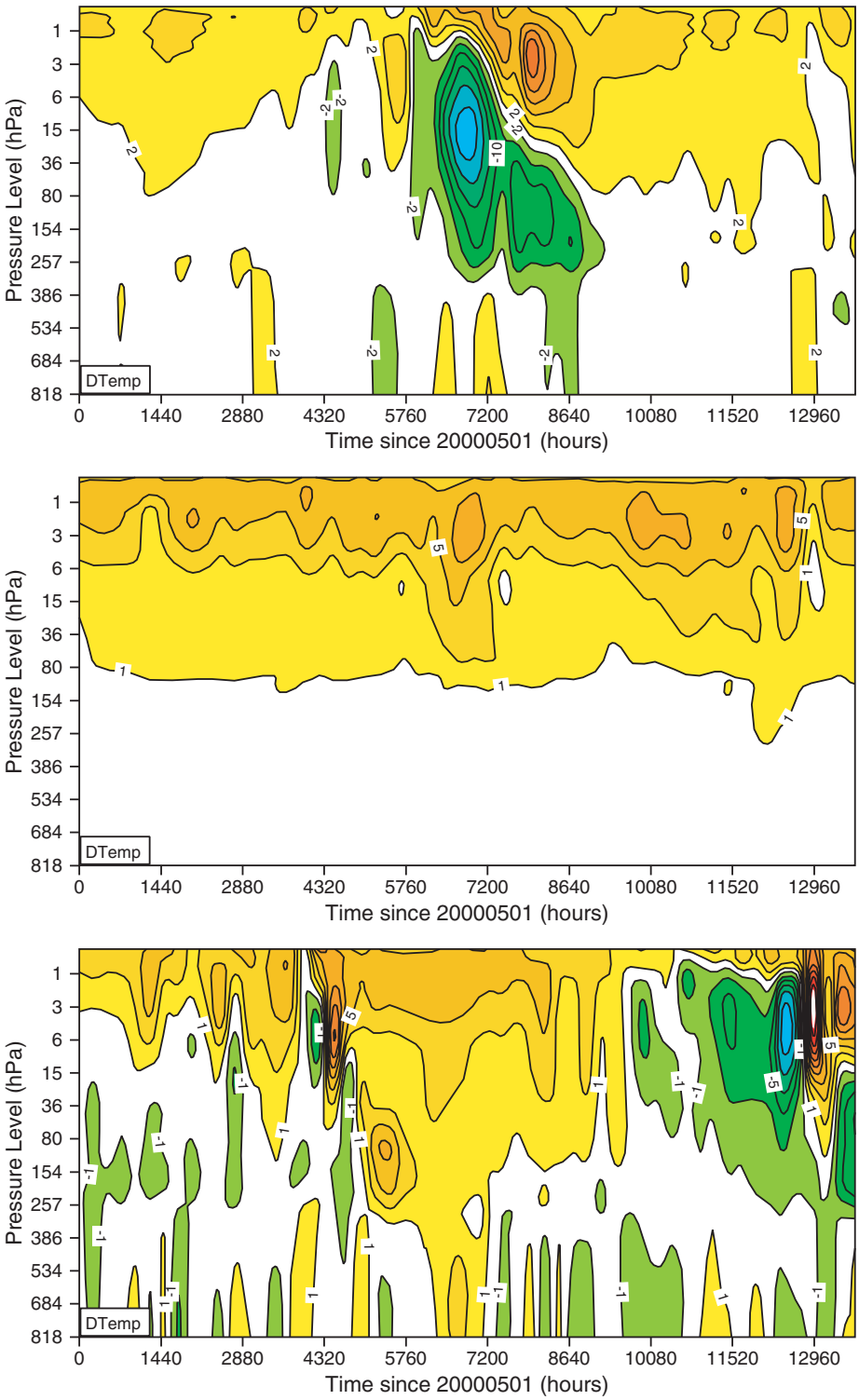

Figure 8 : The time-series of the differences (R6R-R4R) in temperature distribution over the zones 90°N-60°N (top), 30°N-30°S (middle) and 60°S-90°S (bottom), due to a different shortwave radiation scheme. Results are with the T_L159 L60 model running for 19 months from 20000501, with the radiation calculations interactive with the prognostic ozone. Unit is degree K.

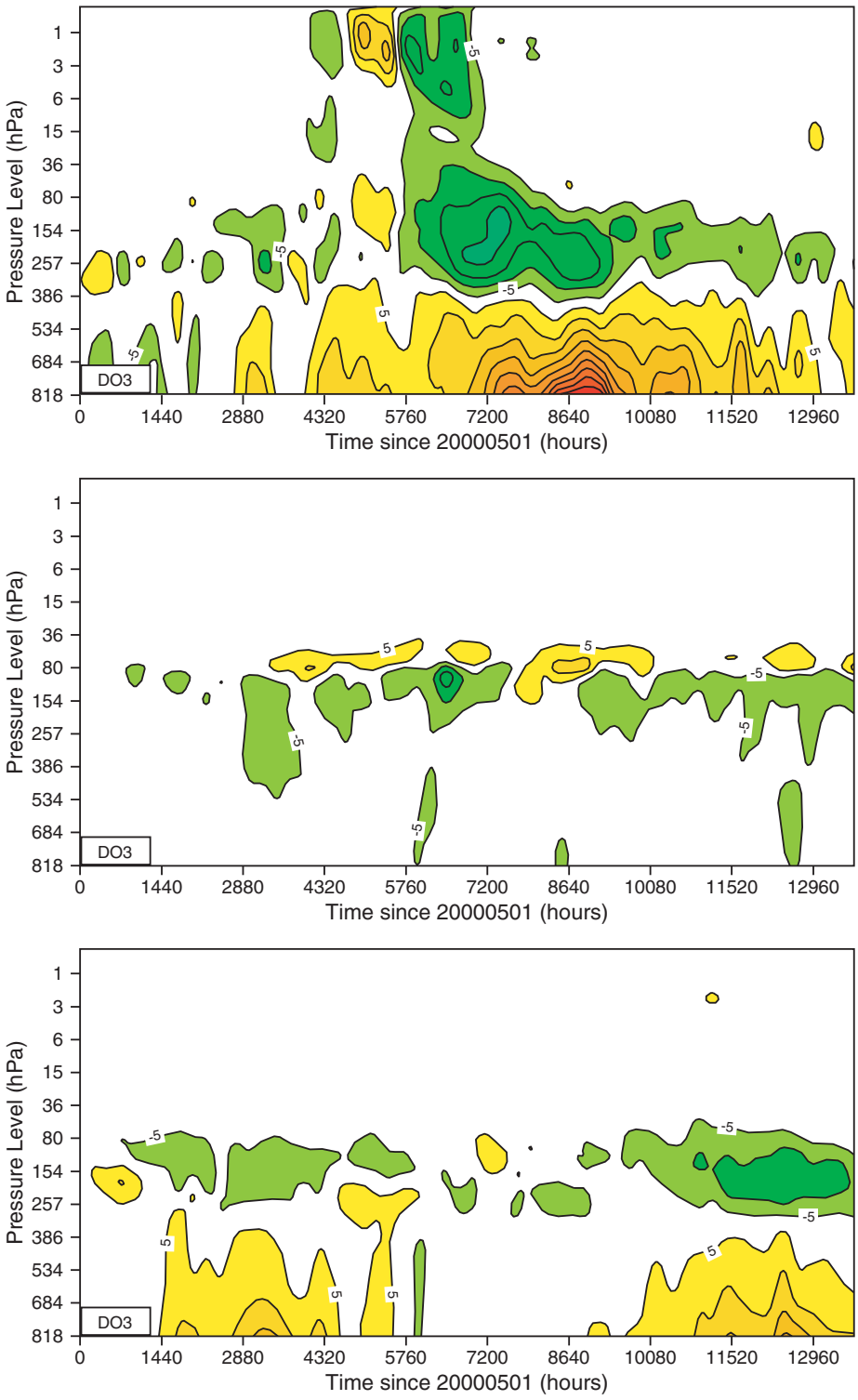

Figure 9 : The time-series of the relative differences ([R6R-D6R]/D6R) in ozone distribution over the zones 90°N-60°N (top), 30°N-30°S (middle) and 60°S-90°S (bottom), due to interactions between prognostic ozone and radiation. Results are with the T_L159 L60 model running for 19 months from 20000501. Unit is percent.

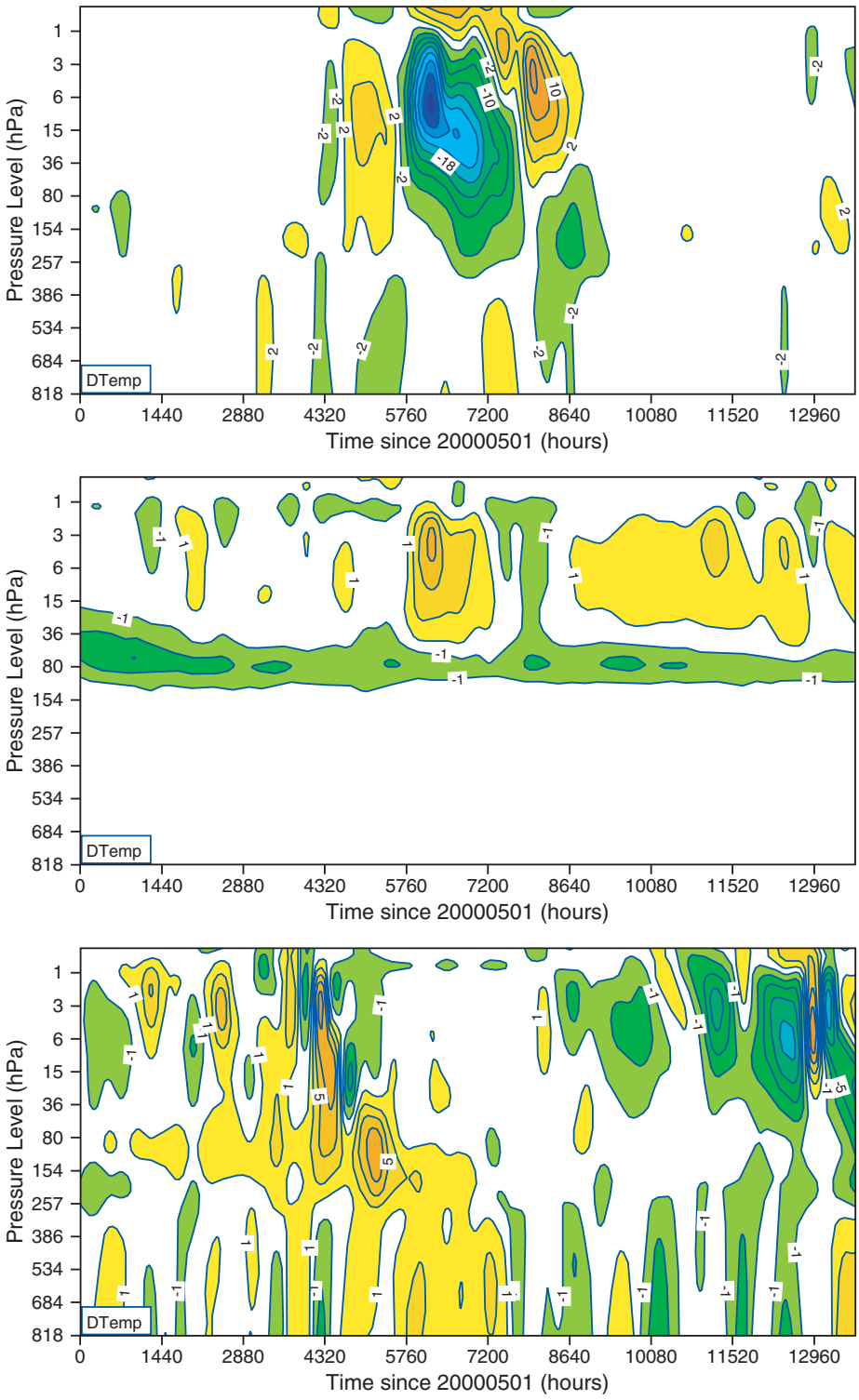

Figure 10 : The time-series of the differences (R6R-D6R) in temperature distribution over the zones 90°N-60°N (top), 30°N-30°S (middle) and 60°S-90°S (bottom), due to interactions between prognostic ozone and radiation. Results are with the T_L159 L60 model running for 19 months from 20000501. Unit is degree K.

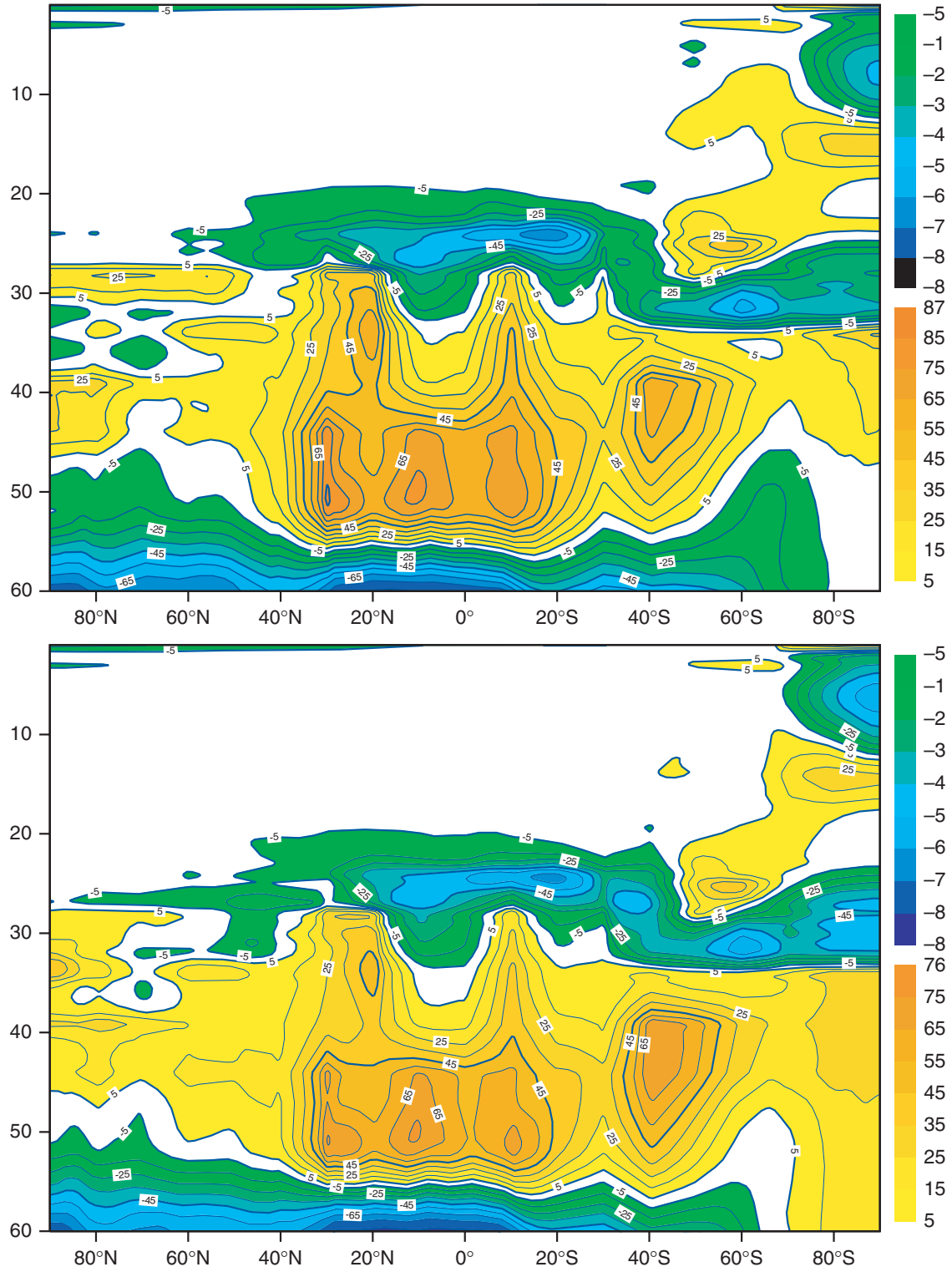

Figure 11 : The relative difference in ozone concentration for the second July of the integrations (in percent). Step is 10 percent starting from -5 and +5 %. Top panel is (D6R-FL)/FL, bottom panel is (R6R-FL)/FL where FL is the ozone climatology from Fortuin and Langematz

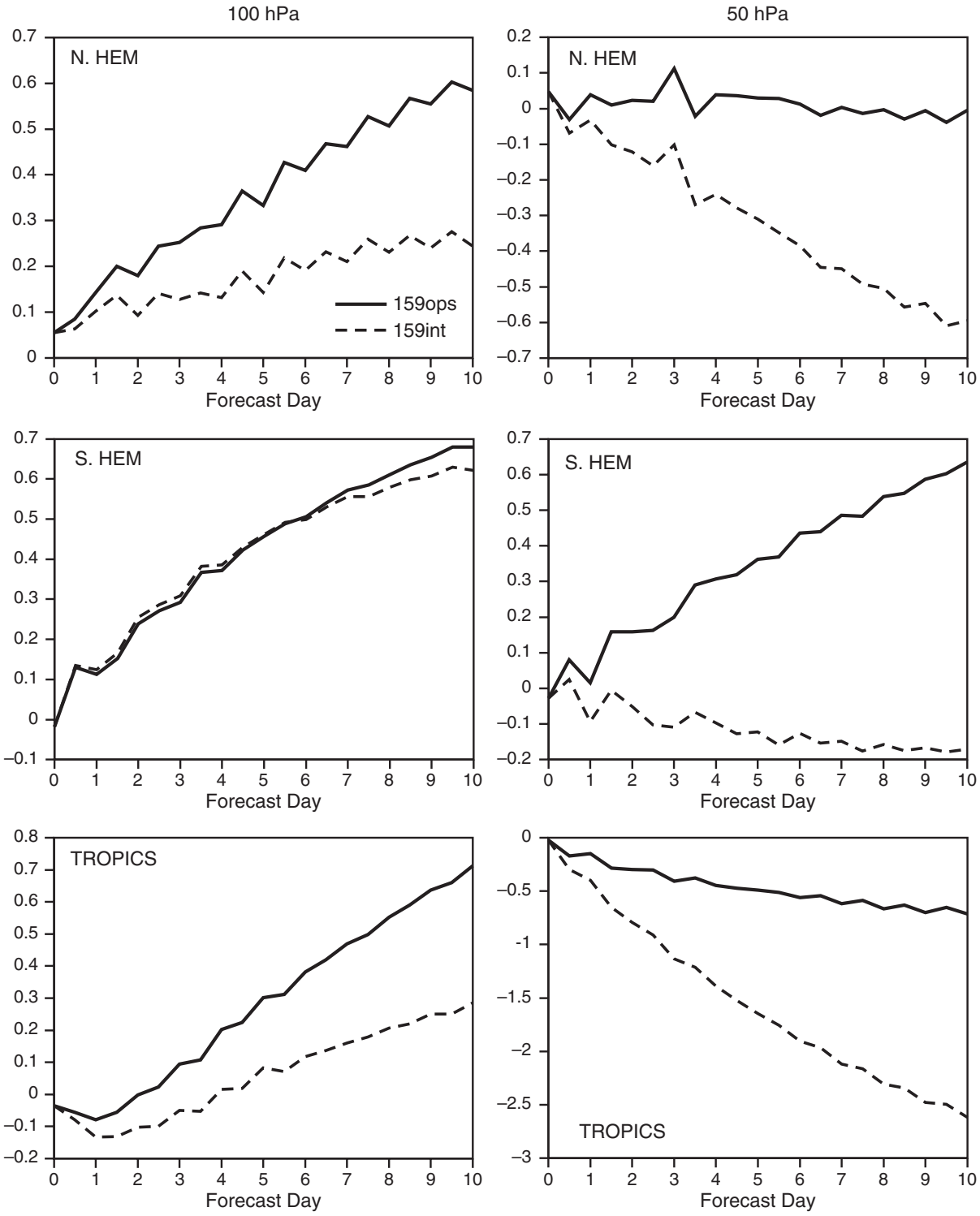

Figure 12 : The mean temperature error at 100 hPa (left) and 50 hPa (right), for the Northern (top panels) and Southern (middle panels) hemispheres, and the 20°N-20°S tropical area (bottom panels) for T_L159 L60 10-day forecasts every second day between 1 January 1992 and 31 March 1992, without (ops) and with (int) radiation interactions with the prognostic ozone field.

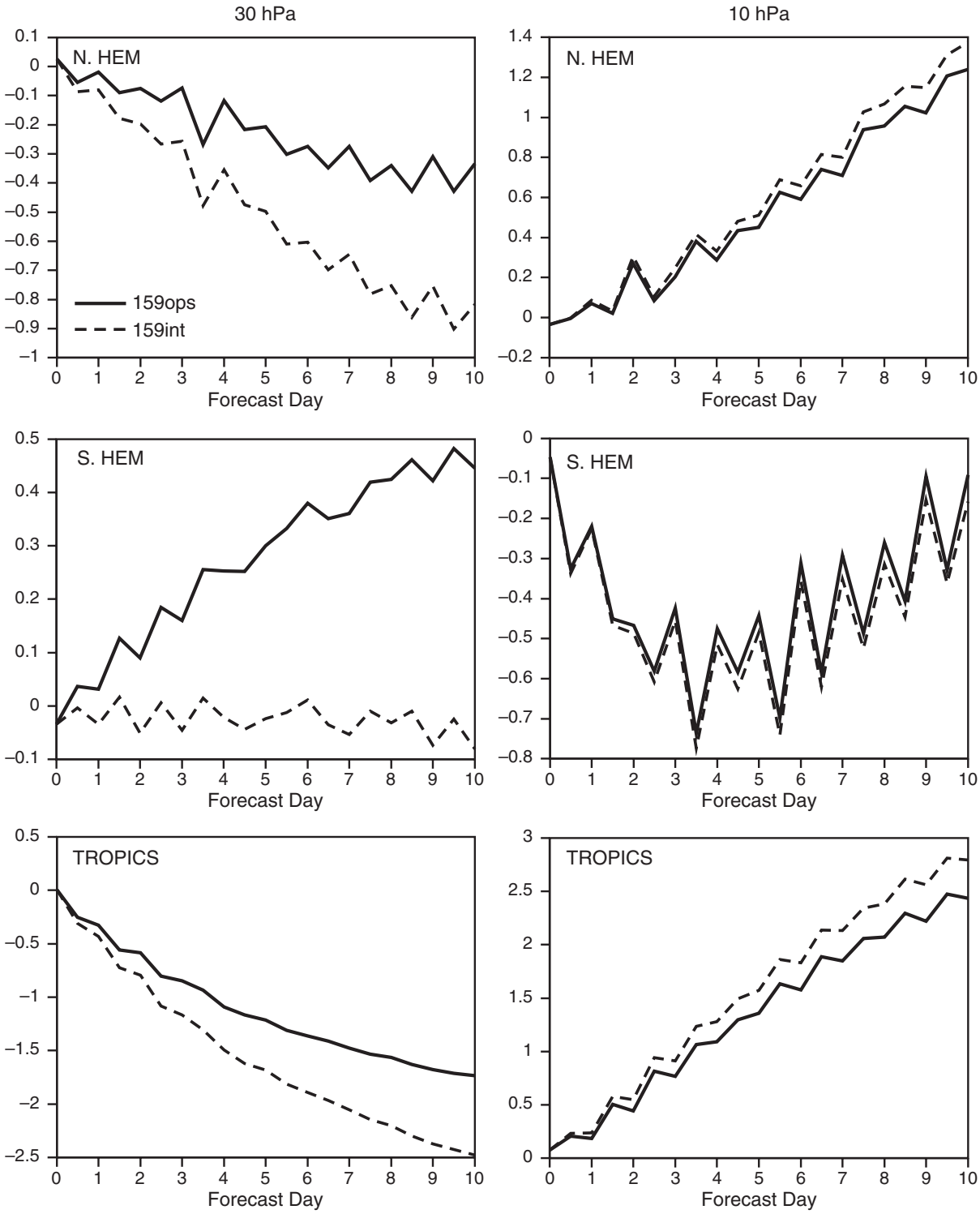

Figure 13 : As in Fig.12, but for the mean temperature error at 30 hPa (left) and 10 hPa (right).

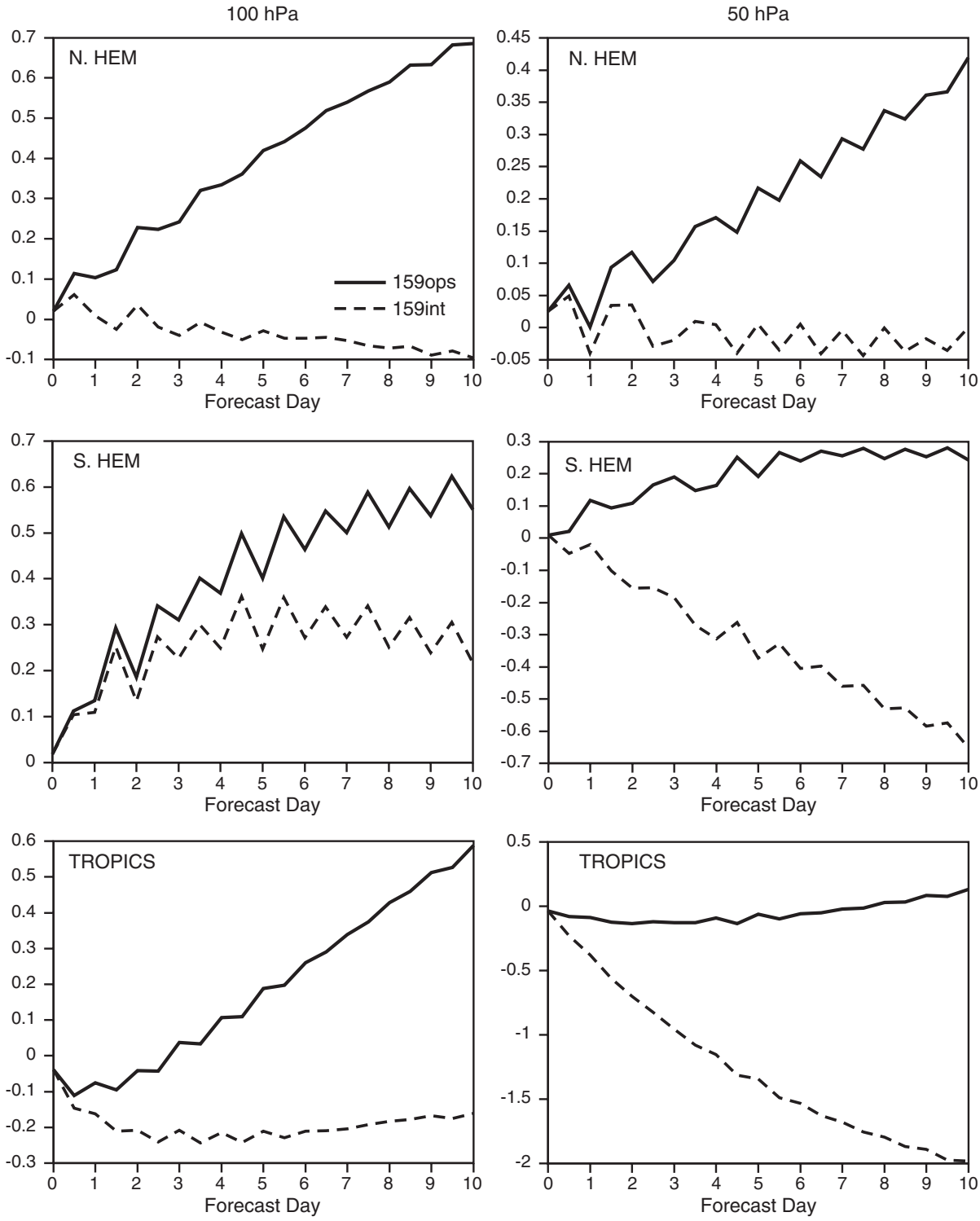

Figure 14 : As in Fig.12, but for T_L159 L60 10-day forecasts every second day between 19930801 and 19931031. Left panels are for 100 hPa, right panels for 50 hPa, top panels for Northern hemisphere, middle panels for Southern hemisphere, and bottom panels for the tropical area.

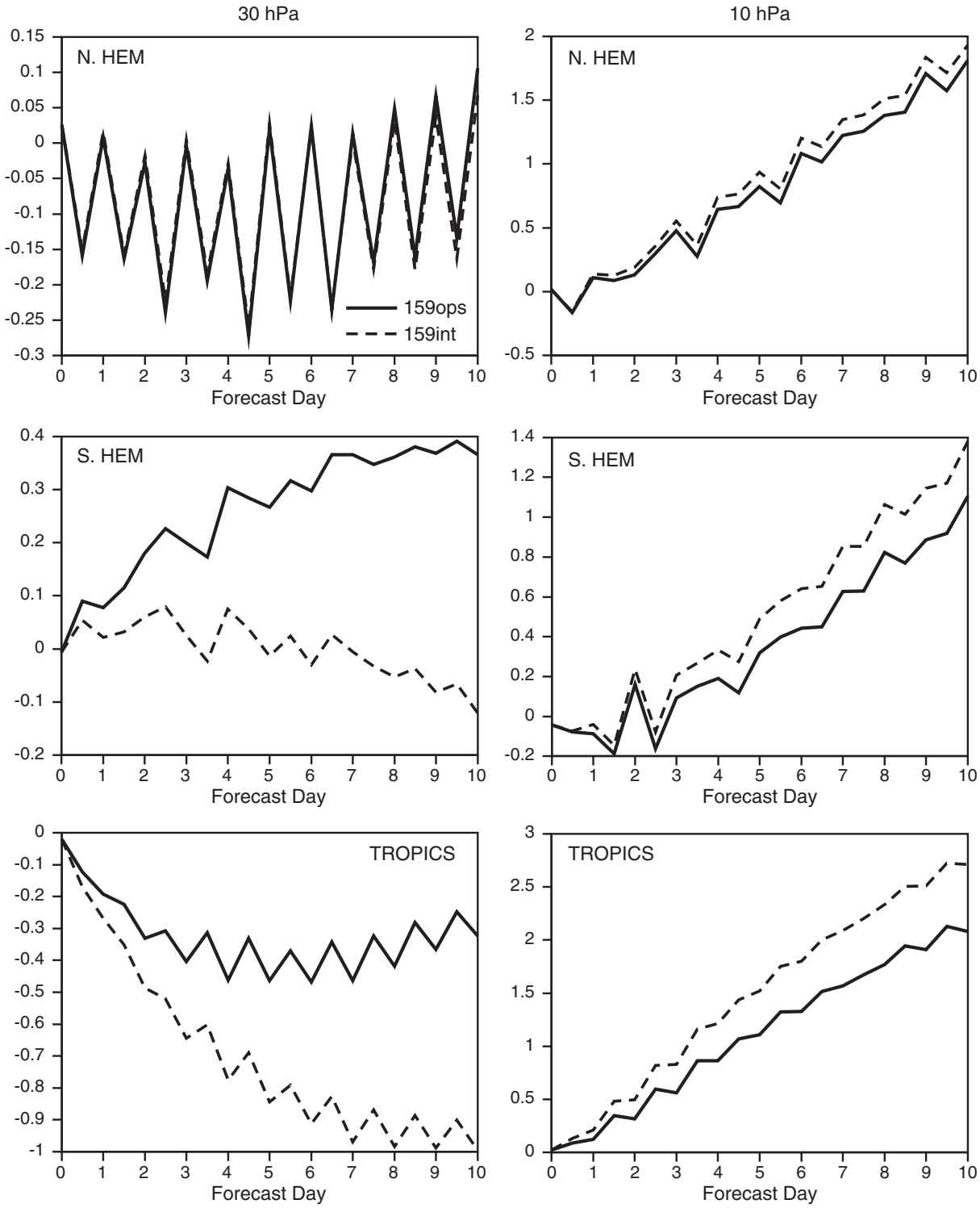

Figure 15 : As in Fig. 14, but for the mean temperature error at 30 hPa (left) and 10 hPa (right).

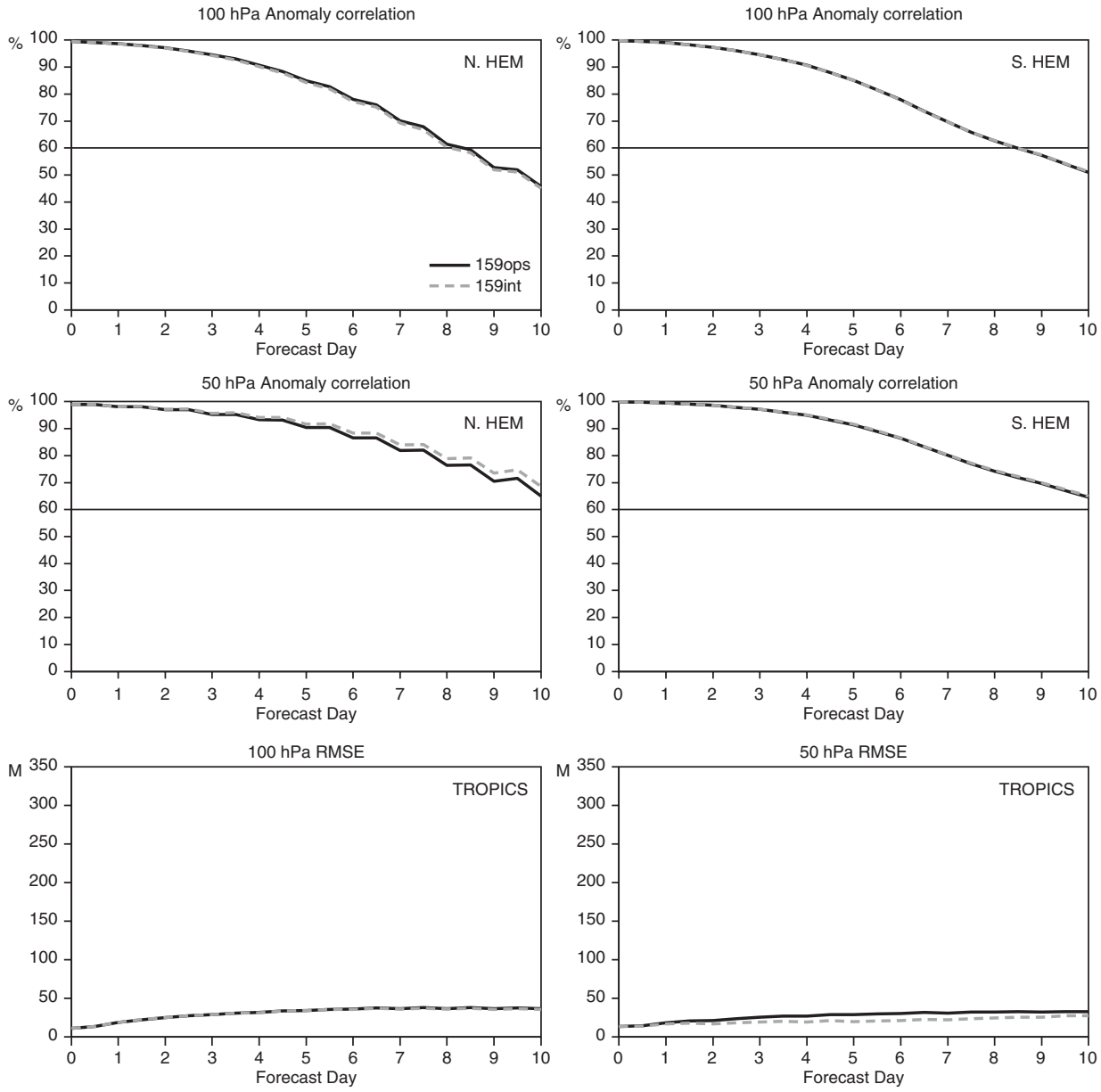

Figure 16 : The anomaly correlation of the geopotential height at 100 and 50 hPa (top and middle panels, respectively) for the Northern (left) and Southern (right) hemispheres. Bottom panel is the r.m.s. error in geopotential height at 100 and 50 hPa in the 20°N-20°S tropical area. Forecasts are for the August to October 1993 period (see Fig. 14). Reference analysis is ERA40.

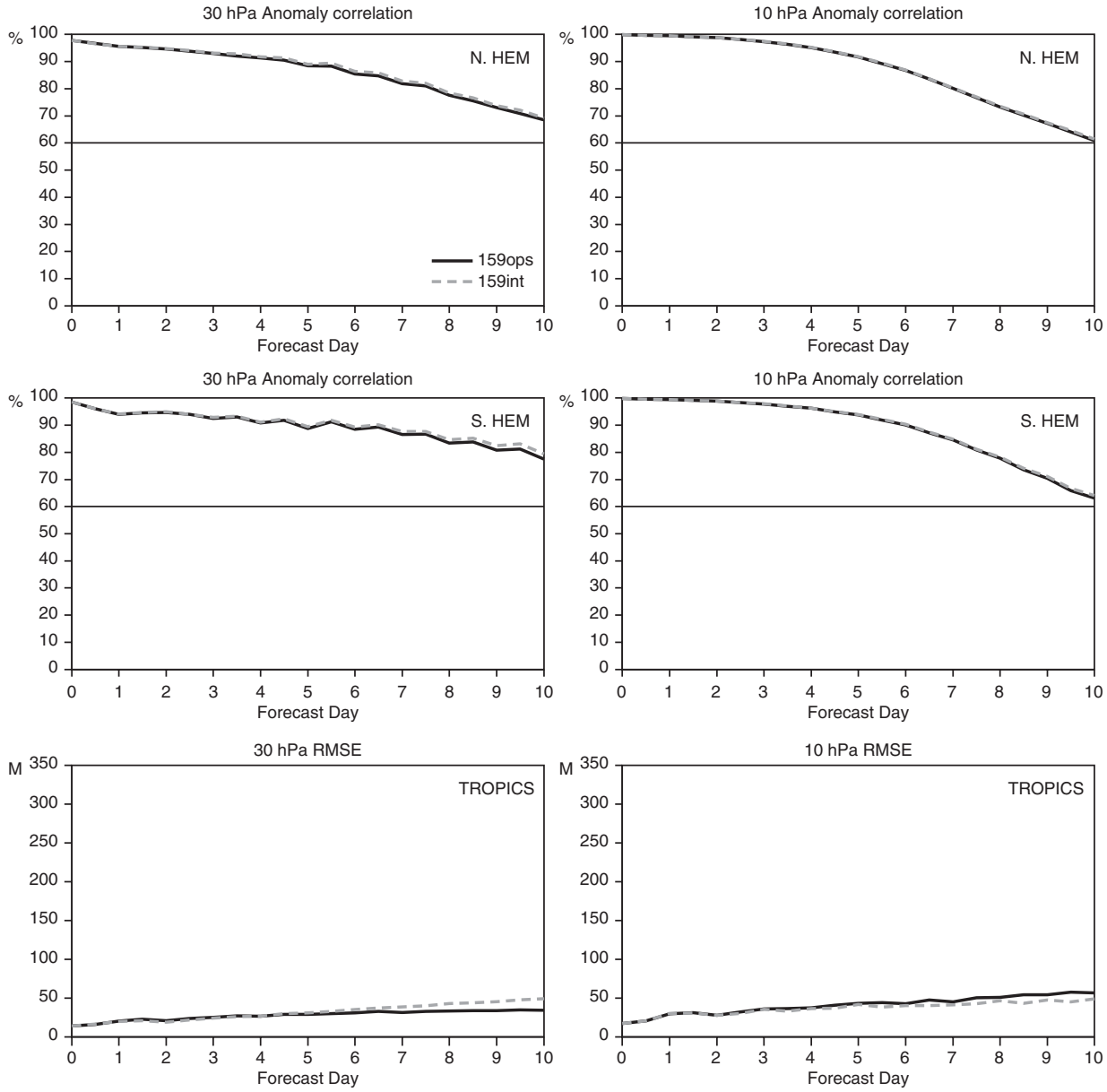

Figure 17 : As in Fig. 16, but for the 30 and 10 hPa pressure levels.

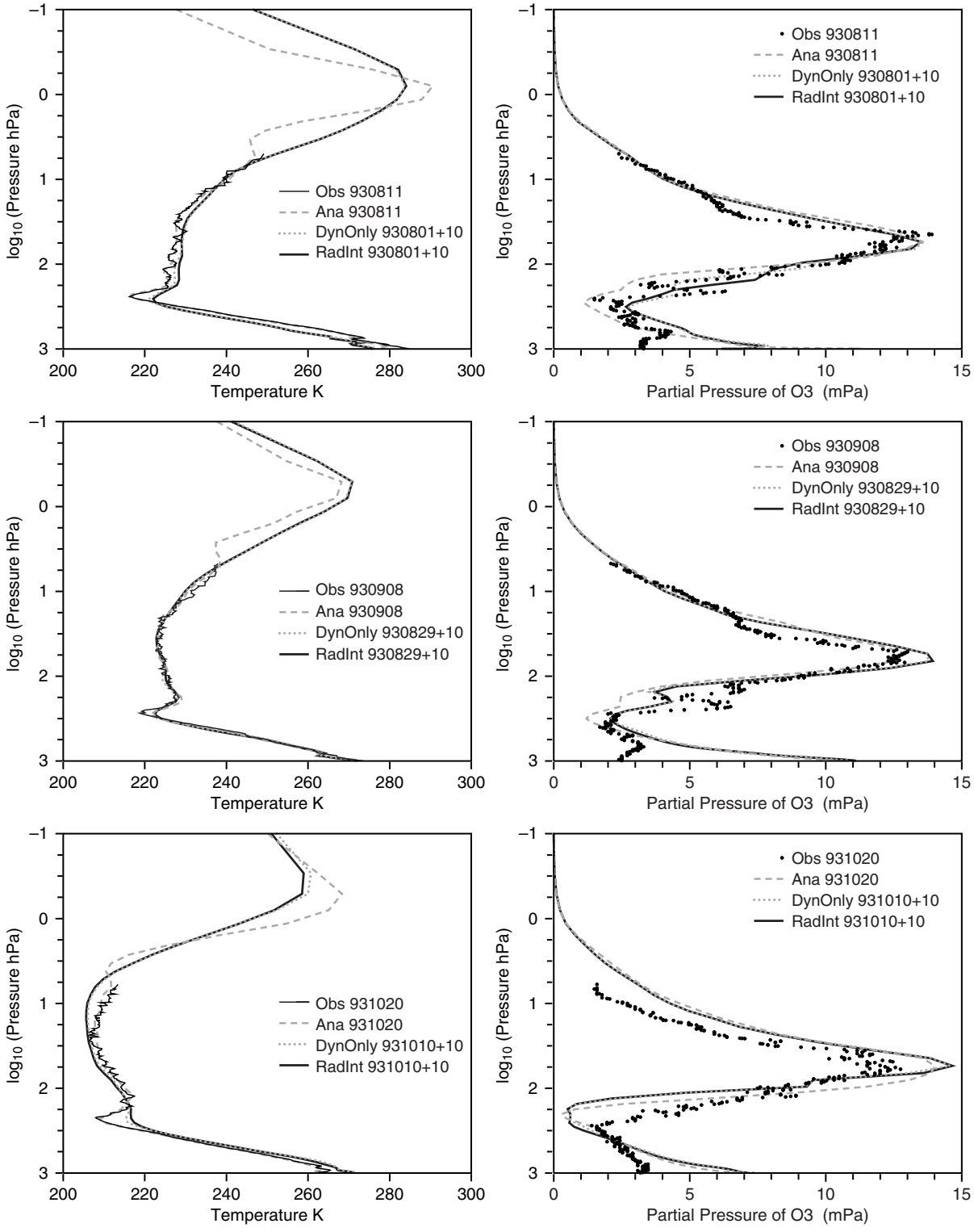

Figure 18 : Temperature (left) and ozone (right) profiles over Ny Alesund on 930811, 930908, and 931020.

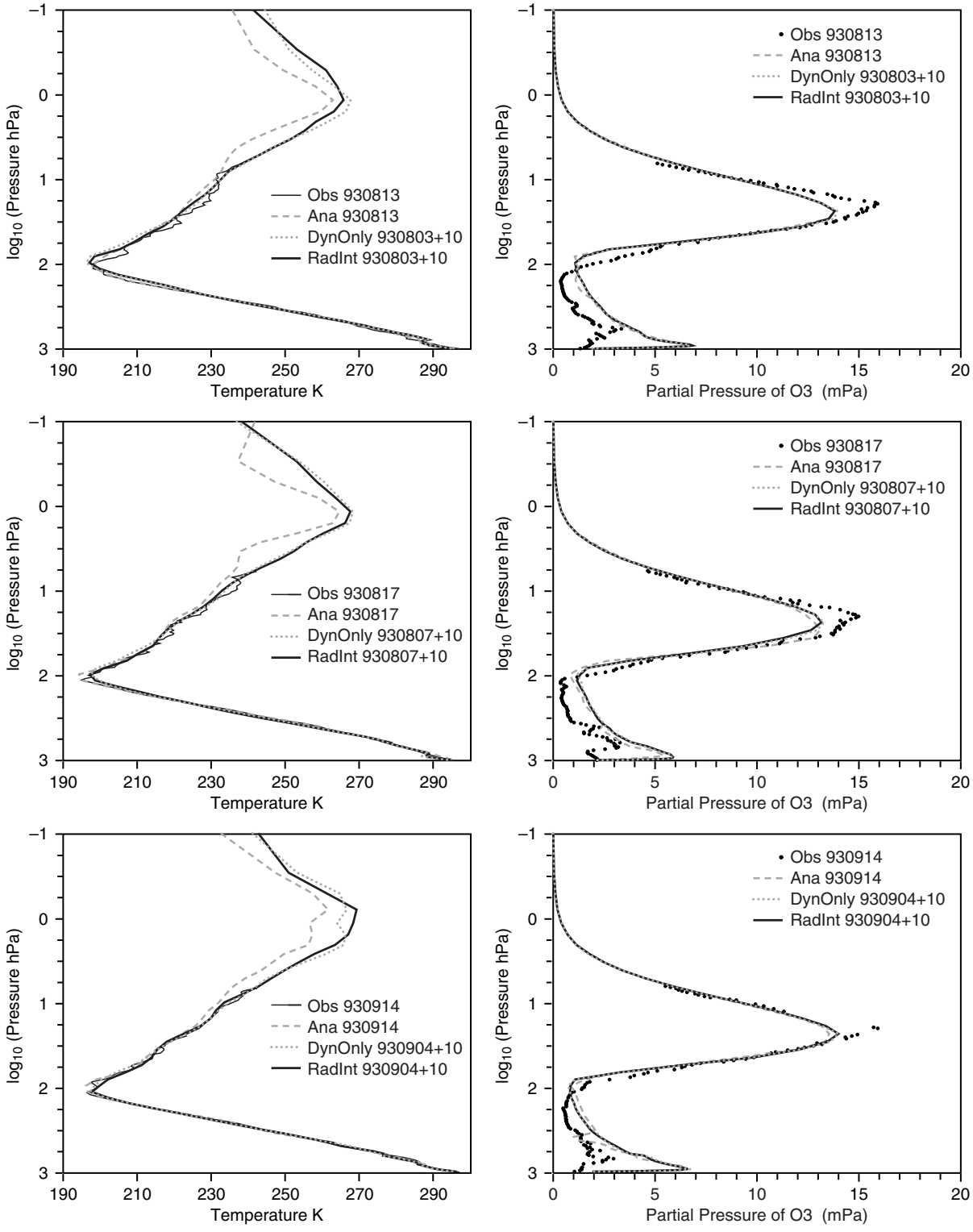

Figure 19 : As in Fig. 18, but for Hilo, Hawaii, on 930813, 930817, 930914.

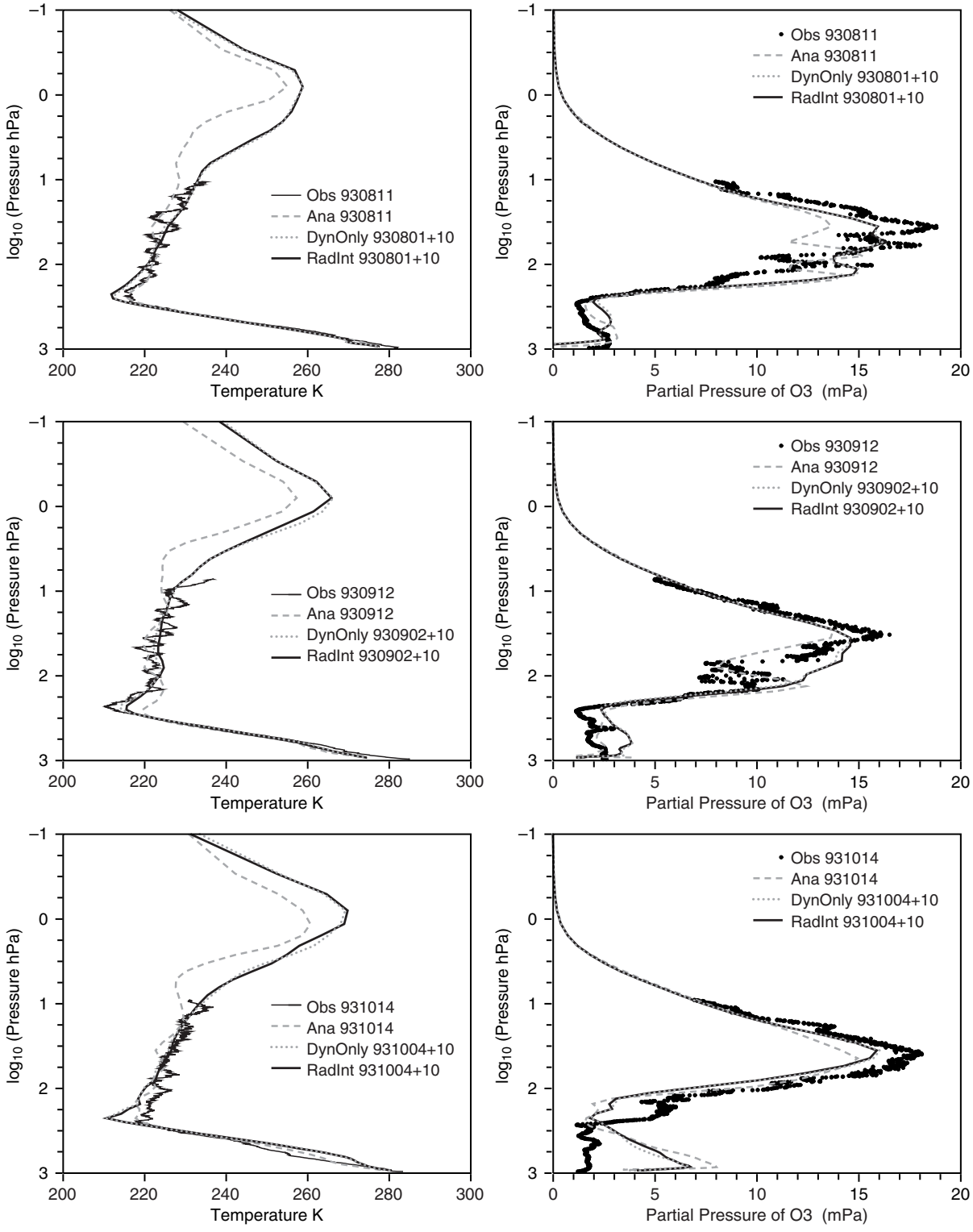

Figure 20 : As in Fig. 19, but for Lauder, NZ, on 930811, 930912, 931014.

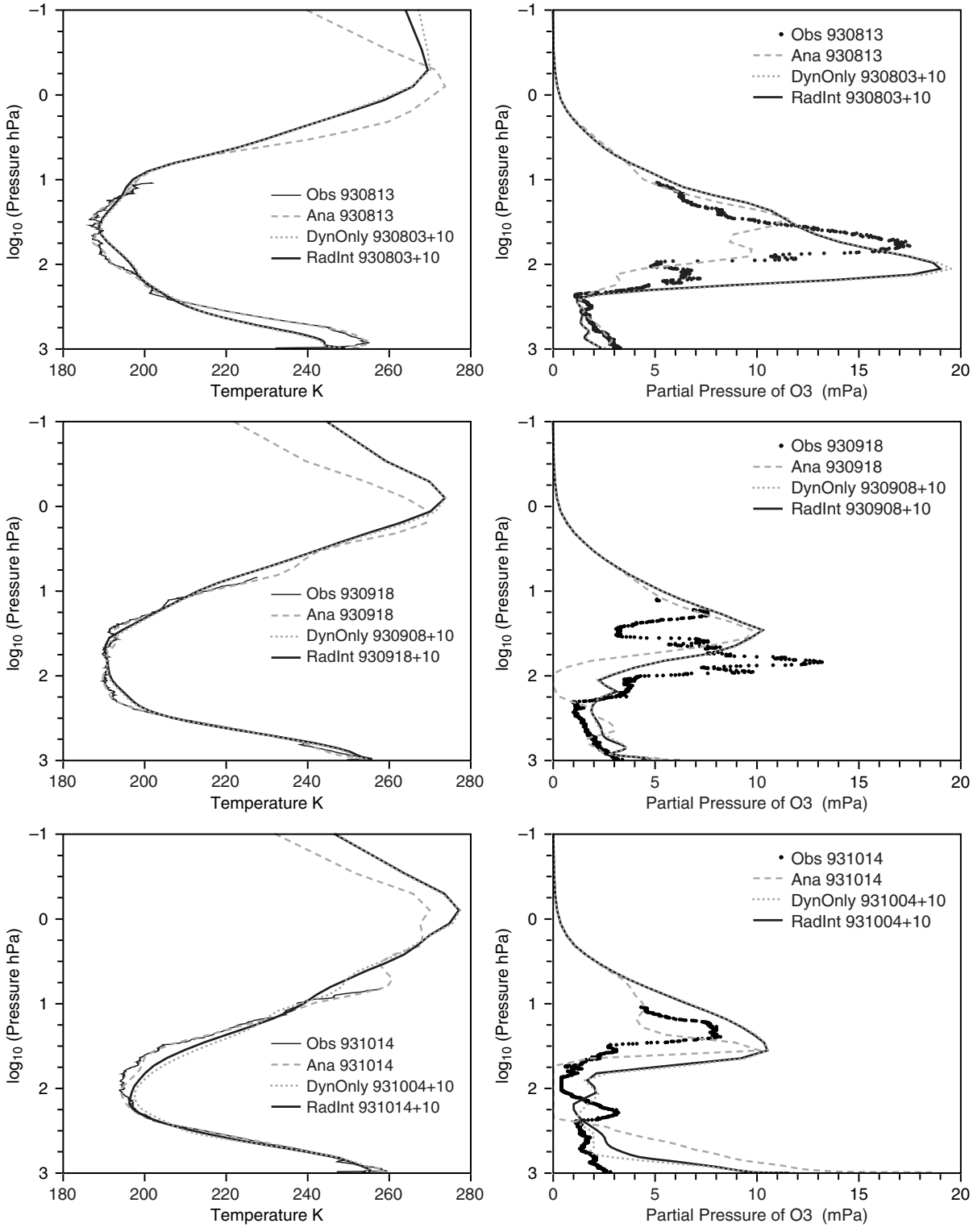

Figure 21 : As in Fig.18, but for Georg von Neumayer on 930813, 930918, and 931014.

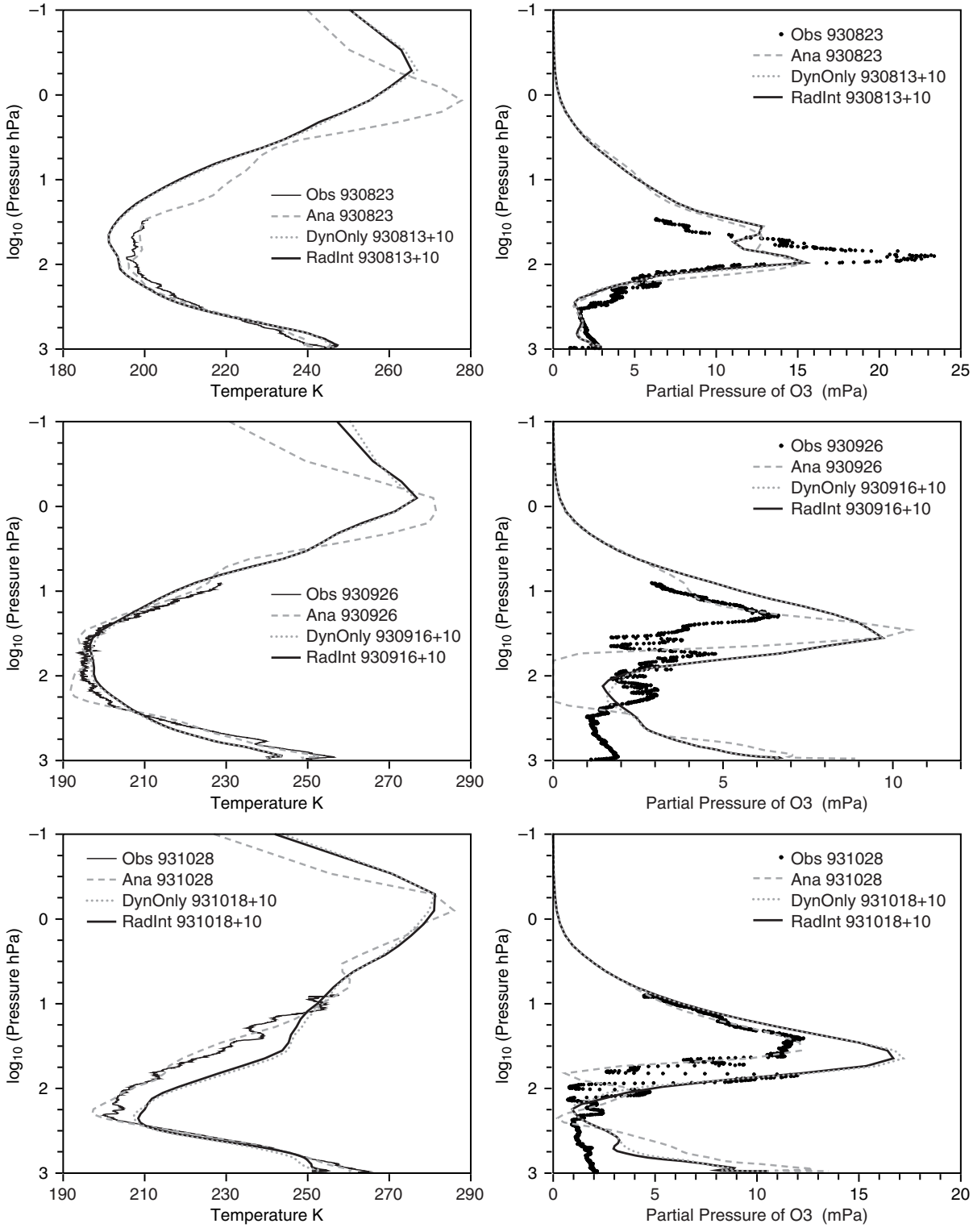

Figure 22 : As in Fig. 18, but for McMurdo on 930823, 930925, 931028.

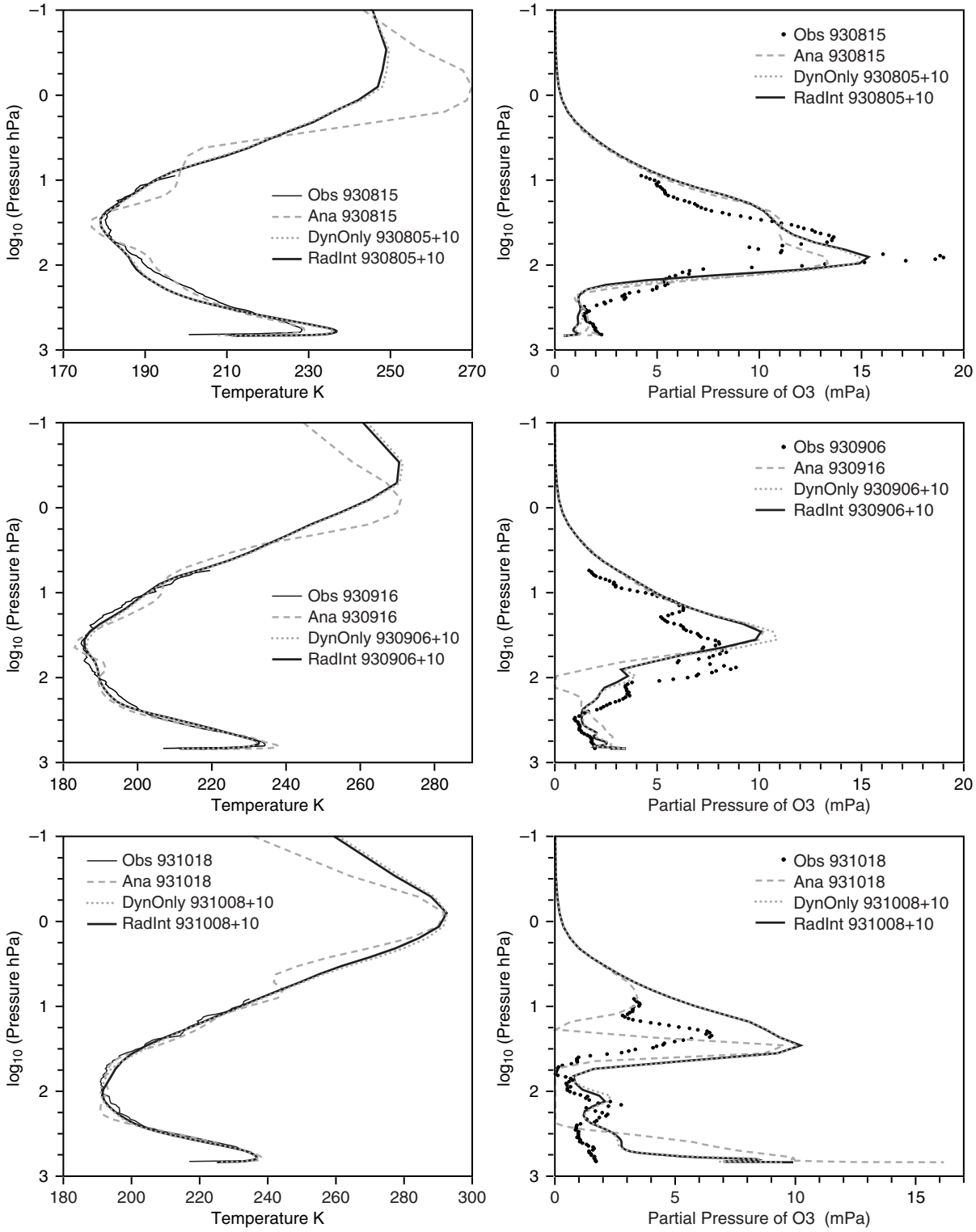

Figure 23 : As in Fig. 18, but for the South Pole on 930815, 930916, and 931018.